Supporting information

A Scalable Approach Using gC_3N_4-Covalent Organic Framework Hybrid Catalyst Towards Sustainable Hydrogen Production from Seawater and Wastewater

Kiran Asokan,[a,b] T. M. Bhagyasree,[a,b] George Devasia,[b,c] Sailaja Krishnamurty,[b,c] Sabah Solim,[d] Lina Rueda,[d] Dhabia M. Al-Mohannadi,[e] Mohammed Al-Hashimi,[e] Konstantinos Kakosimos,[e] and Sukumaran Santhosh Babu*[,a,b]

[a]Organic Chemistry Division, National Chemical Laboratory (CSIR-NCL), Dr. Homi Bhabha Road, Pune-411008, India

[b]Academy of Scientific and Innovative Research (AcSIR), Ghaziabad-201 002, India

[c]Physical and Materials Chemistry Division, National Chemical Laboratory (CSIR-NCL), Dr. Homi Bhabha Road, Pune-411008, India

[d]Qatar Shell Research & Technology Centre, Qatar Science & Technology Park, Education City, Doha, Qatar

[e]Chemical Engineering Department, Texas A&M University at Qatar, Doha, Qatar

*Correspondence: sb.sukumaran@ncl.res.in

Table of Contents

Materials and Methods

1,3,5-Triformyl phloroglucinol (**Tp**) was purchased from Hygeia laboratories, Pune, India. *p*-Phenylene diamine (**Pa**) and *p*-toluenesulfonic acid (PTSA) were purchased from Tokyo Chemical Industry, India. Deionized water, methanol, and dichloromethane were used for washing COF. Synthesized COFs were characterized with Fourier transform infrared spectroscopy (FT-IR) in KBr mode using a Bruker Alpha-E Infrared spectrophotometer, and the wavenumbers of the recorded IR signals are quoted in cm^{-1}. Wide-angle X-ray diffraction (WAXD) analysis was recorded on a Rigaku MicroMax-007HF equipped with a high-intensity microfocus rotating anode X-ray generator. The data were collected with the help of Control Win software. A Rigaku, R-axis IV++ detector was used for the wide-angle experiments using Cu K-alpha (1.54 Å) radiation outfitted with a Ni filter, and an aluminum holder was used as the sample holder. Thermogravimetric analysis (TGA) of the samples was carried out in a PerkinElmer STA 600 analyser in a N_2 atmosphere by maintaining a temperature ramp between room temperature and 900 °C with a heating rate of 10 °C min^{-1}. Prior to analysis, samples were activated at 100 °C to remove solvents and moisture trapped in pores. BET adsorption experiments (up to 1 bar) of COF samples were performed on a Quantachrome Quadrasorb/Autosorb automatic volumetric instrument. Prior to surface area analysis, the samples were activated at 130 °C for 24 hours. The porosity of the samples was measured by N2 adsorption of an activated sample at 77 K. The average pore diameter of the samples was calculated by nonlocal density functional theory (NLDFT). The Brunauer–Emmett–Teller (BET) surface area of the samples was determined by multipoint BET analysis. The photocatalytic experiments were carried out using a Holmarc solar simulator, and the quantification of H2 gas was performed using a NUCON gas chromatograph 5700 model.

All the DFT calculations were performed under periodic boundary conditions using Vienna ab initio Simulation Package (VASP).[S1] The generalized gradient approximation (GGA) employed with Perdew-Burke-Ernzerhof (PBE)[S2] was used as an exchange correlation function. The projector augmented wave (PAW) method was used to describe ion-electron interactions. The kinetic energy cutoff was set to 400 eV. DFT-D3 method of Grimme was incorporated to take into account of long-range van der Waals (vdW) interactions.[S3] A vacuum space of 20 Å along Z axis was selected to avoid unwanted interactions with a Monkhorst Pack k-point grid of 1 × 1 × 1. The convergence criteria for energy were set to be 10-6 eV and optimization was carried out until the forces converged to 0.005 eV $Å^{-1}$.

I. Experimental Procedure for Photocatalytic HER Experiments

Photocatalytic HER experiments were carried out under steady-state conditions by headspace analysis at room temperature (25 ^{o}C). The catalyst was dispersed in water with SED by sonication for 30 min, and subsequently, Argon gas was bubbled for 30 min to remove any dissolved oxygen. During the reaction, the entire suspension is stirred by using a magnetic stirrer. In general, 5 mg of the photocatalyst was suspended in an airtight quartz round bottom flask (closed with a silicone rubber septum) of 50 mL capacity containing 20 mL distilled water and 200 mg ascorbic acid. The reaction's progress was monitored by illuminating various visible light sources such as solar simulator, and sunlight. The reactor's headspace was periodically sampled with an offline injection system by a gas phase syringe having an injection volume of 500 μL. The gas analysis was carried out by regular sampling every hour, and a gas chromatograph (GC) equipped with a TCD detector (Nucon engineers) was employed for quantitative analysis. After a saturation regime in the first cycle, the photocatalyst suspension is purged with Ar for 30 min before starting the next cycle, and for repeated experiments, the catalyst is filtered after each photocatalytic cycle, washed with excess water and methanol, and dried under vacuum.

The photocatalytic experiments were carried out using Holmarc made solar simulator and quantification of H_2 gas was done using NUCON gas chromatograph 5700 model.

Stability tests for photocatalysts: At first, the weight loss of the catalyst after each photocatalytic reaction cycle is checked, and found negligible mass loss or gain. The decomposition of the catalyst under reaction conditions for a long time was also tested, and no other gases, except H_2 could be detected by GC. The structural stability of the catalyst over time is monitored by FT-IR and solid-state HR-TEM, and XPS analysis. The consistency in the rate of H_2 evolution is closely monitored with repeated cyclic experiments over 5 cycles.

The AQY of catalyst were calculated using irradiation under monochromatic light sources of different wavelength. For this 450, 500 and 550 nm were chosen and calculated using the following equations.

$$AQY = \frac{\boldsymbol{Amount\ of\ product\ obtained}}{\boldsymbol{number\ of\ incident\ photons}} \times \mathbf{100}$$

$$= \frac{n_p \times N_A \times n \times h \times C}{P \times S \times \lambda} \times 100$$

Where, n_p is the H_2 evolution rate (mol s^{-1}), N_A is Avogadro constant (6.022×10^{23} mol^{-1}), n is number of transferred electrons in hydrogen evolution reaction (2), h is the Planck constant (6.626×10^{-34} J·s), C is the speed of light (3×10^{8} $m\cdot s^{-1}$), P is the intensity of irradiation light ($W\cdot m^{-2}$), S is the irradiation area (m^2), λ is the wavelength of the monochromatic light (m).

II. Photoelectrochemical Experiments

Electrochemical impedance spectroscopy (EIS) measurements were carried out in a CH electrochemical workstation in a standard three-electrode electrochemical cell with working electrode as catalyst coated FTO plate, a platinum plate as the counter electrode, and a saturated Ag/AgCl electrode as the reference electrode. A sodium sulfate solution (0.2 M) was used as the electrolyte. Preparation of the working electrode: 2 mg of catalyst powder was mixed with 1.0 mL ethanol and 10 μL Nafion D-520 dispersion solutions (5.0 %) and sonicated for 30 minutes. The resulting mixture was deposited evenly on the bottom 1×1 cm^2 area of the FTO glass plate conducting surface (confirmed by digital multimeter) and left in the air to dry.

Photocurrent-time (I-T) measurement: Current measured in chronoamperometry mode in a fixed potential of 0.9 V, FTO electrode mounted approximately 45^o angle closer to the counter electrode, a visible light irradiation solar simulator (AM 1.5G, 100 mW cm^{-2}).

Transmission Electron Microscope (TEM): The samples for TEM were prepared by drop-casting the 2D polymer dispersions in the EtOH on a carbon-coated Cu grid and allowed to dry overnight in desiccators.

III. Synthesis and Characterization

Synthesis of PVP-Pt NPs.

Polyvinylpyrrolidone-coated Pt nanoparticles (PVP-Pt NPs) were synthesized according to the reported literature.[S4] In a typical procedure, 5.36g of 0.4 wt% H_2PtCl_6 aqueous solution was added to a 15 mL beaker. To that, 3 mL of 0.442 g/mL PVP (MW 30,000) was diluted with 9 mL of deionized water and added to the beaker. Further, Sodium borohydride solution was

used to reduce Pt (IV) into metallic nanosize Pt particles. 0.1 g of $NaBH_4$ was dissolved in 50 mL water and the solution was added dropwise to a solution consisting of H_2PtCl_6 and PVP. The amount of sodium borohydride required was monitored by a UV-visible spectrometer until all the Pt (IV) ions were reduced to platinum metal. With the addition of sodium borohydride, the H_2PtCl_6 peak at 270 nm gradually disappears, indicative of a complete reduction of Pt (IV). The pH of the solution was adjusted to 5.300 by adding ammonium sulfite. The resulting polymer-stabilized solution had a dark brown color. HR-TEM images of synthesized NPs were analyzed and found to be spherical in shape with a diameter of 2-4 nm.

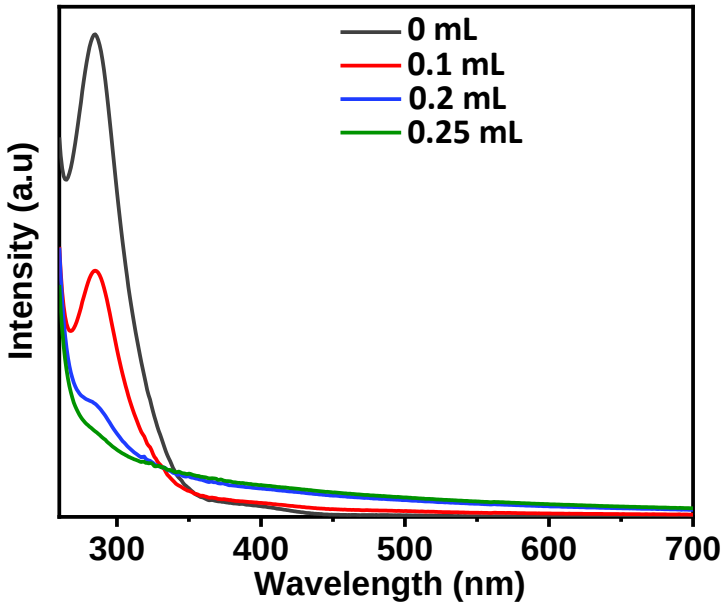

UV-visible absorption spectra of PVP-coated Pt nanoparticles with the addition of reducing agent $NaBH_4$. Complete quenching of the peak was observed after adding 0.25 mL of $NaBH_4$.

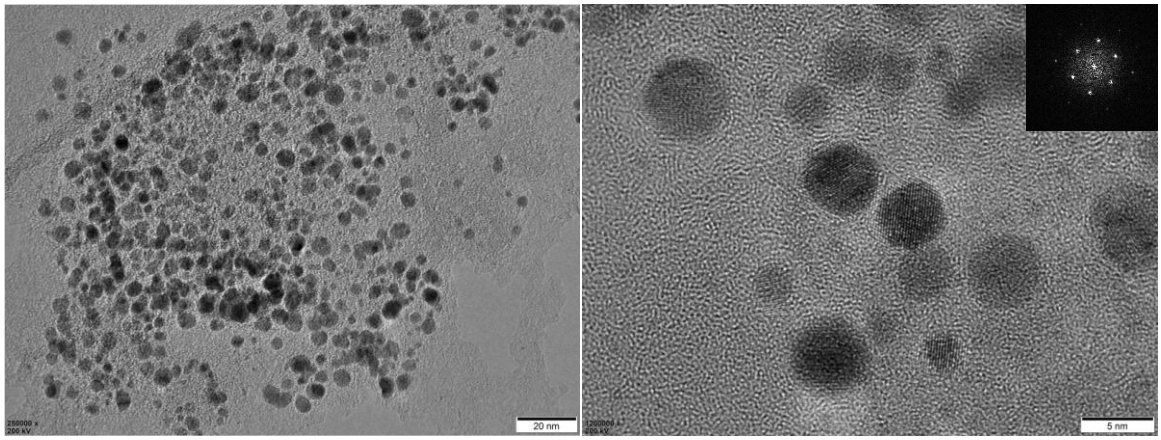

HR-TEM images of **PVP-Pt** nanoparticles synthesized.

Synthesis of gC_3N_4

gC_3N_4 was synthesized, as reported earlier, from a urea precursor.[S5] In a typical procedure, 30 g of urea was taken in a silica crucible and appropriately covered with a lid. It was then heated at 600 °C for 4 hours at 5 °C/min ramping and then allowed to cool slowly. After cooling to room temperature, it was washed with deionized water, 1 N HCl, and ethanol and dried in a vacuum oven at 100 °C for 12 hours

Synthesis of TPG-xs

The synthesis of **TPG-x**s was achieved by the mechanochemical method. In general, PTSA (2.5 mmol, 8 eq.) and **Pa** (0.45 mmol, 1.5 eq.) were ground thoroughly for 10-15 minutes. To that, **Tp** (0.3 mmol, 1 eq.) was added and ground into the mixture, followed by the addition of 50-100 µL water (depending upon the requirement for making the mixture like a paste or jelly kind of material). The grinding was continued for 20 minutes. To the paste, different weight percentages of **gC_3N_4** (x = 10, 25, 50, 75, 100, where x is the weight percentage of **gC_3N_4** to the total quantity of **Tp** and **Pa**) were added and ground for 10-15 minutes. The resulting powder was transferred to a glass vial, closed, and heated at 90 °C for 12 hours. It was then washed using the Soxhlet apparatus with water, methanol, and CH_2Cl_2. The final product was dried in a vacuum oven at 120 °C for 12 hours.

Synthesis of TPG-75

The synthesis of **TPG-75** was performed by the following procedure. 6.6 g of PTSA and 772 mg **Pa** were ground using a mortar pestle for 10 minutes until it became a homogenous mixture. To that, 1 g of **Tp** was added and ground again for 10 minutes. After ensuring a homogenous mixture formation, 100 µL of H_2O was added and ground again for 10 minutes. To the paste, 1.32 g of **gC_3N_4** was added and again ground for 10 minutes. Finally, the mixture obtained was transferred into a glass vial and heated at 90 ^oC for 12 hours followed by Soxhlet washing using H_2O, Methanol. and dichloromethane. After washing the powder was dried in a vacuum oven at 120 ^oC for 12 hours yielding 2.8 g (92 % yield).

Bulk Scale Synthesis of TPG-75-20G

The bulk-scale synthesis of **TPG-75** was performed by using a planetary mixer (Scheme S1, Table S1). Firstly, **Pa** and PTSA were taken in a container and mixed in a planetary mixer for 10 minutes at 1500 rpm. Later, **Tp** was added and again mixed for 10 minutes at the same rpm. After proper mixing of starting materials was confirmed, H_2O was added and mixed at a lower rpm (1000) to ensure homogenous mixing for 10 minutes. To that, **g**$\mathbf{C_3N_4}$ and H_2O were added and mixed again for 10 minutes at 1000 rpm. Finally, H_2O was again added, and mixed the whole mixture at 1500 rpm for 10 minutes. The mixture was transferred into a petri dish and heated at 90 ^oC for 12 hours. The resultant mixture was washed and dried as mentioned earlier. 20 g, 92 % yield.

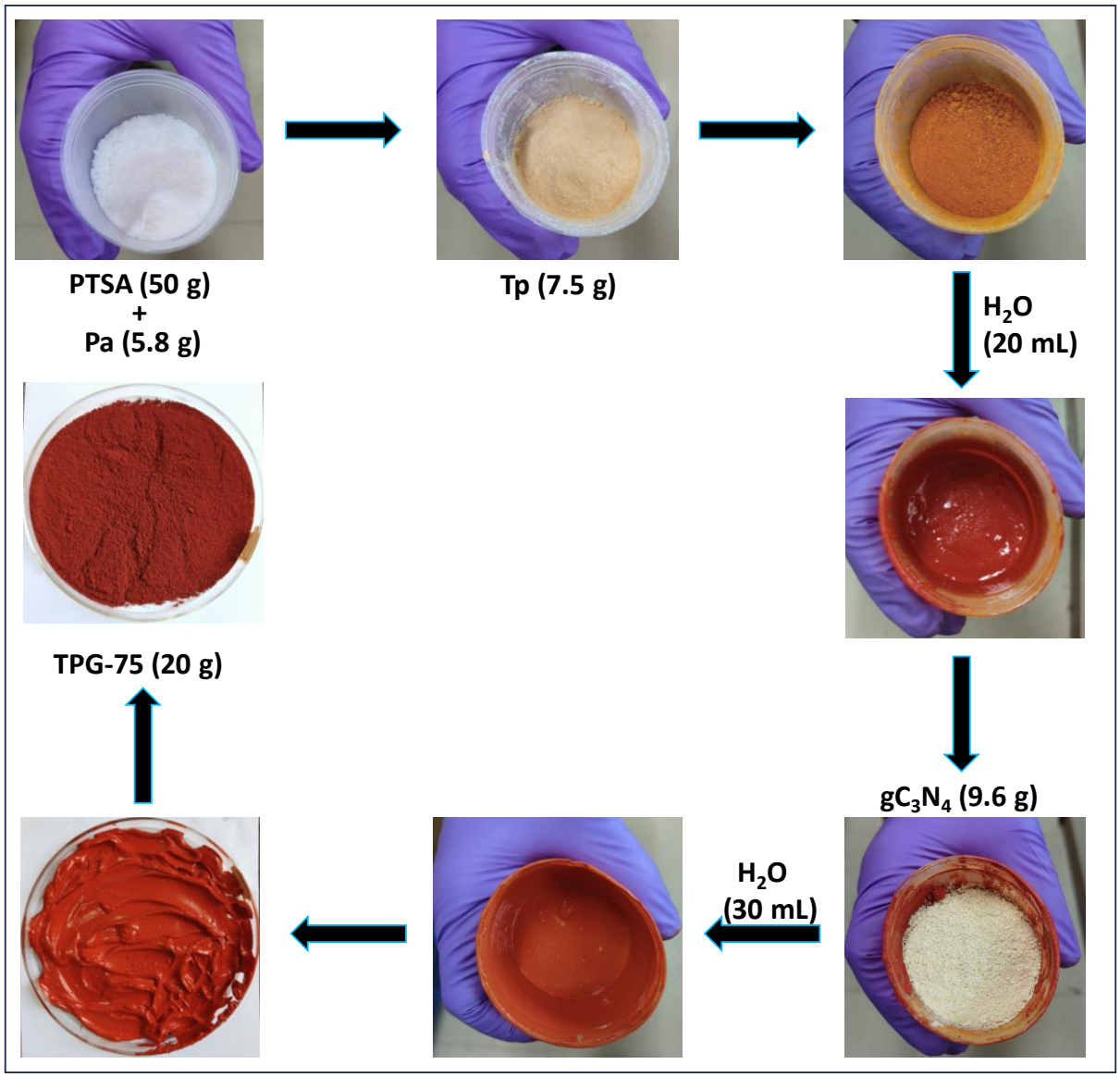

Scheme S1. The bulk scale synthesis scheme of **TPG-75-20G** using the planetary mixer.

Figures and Tables

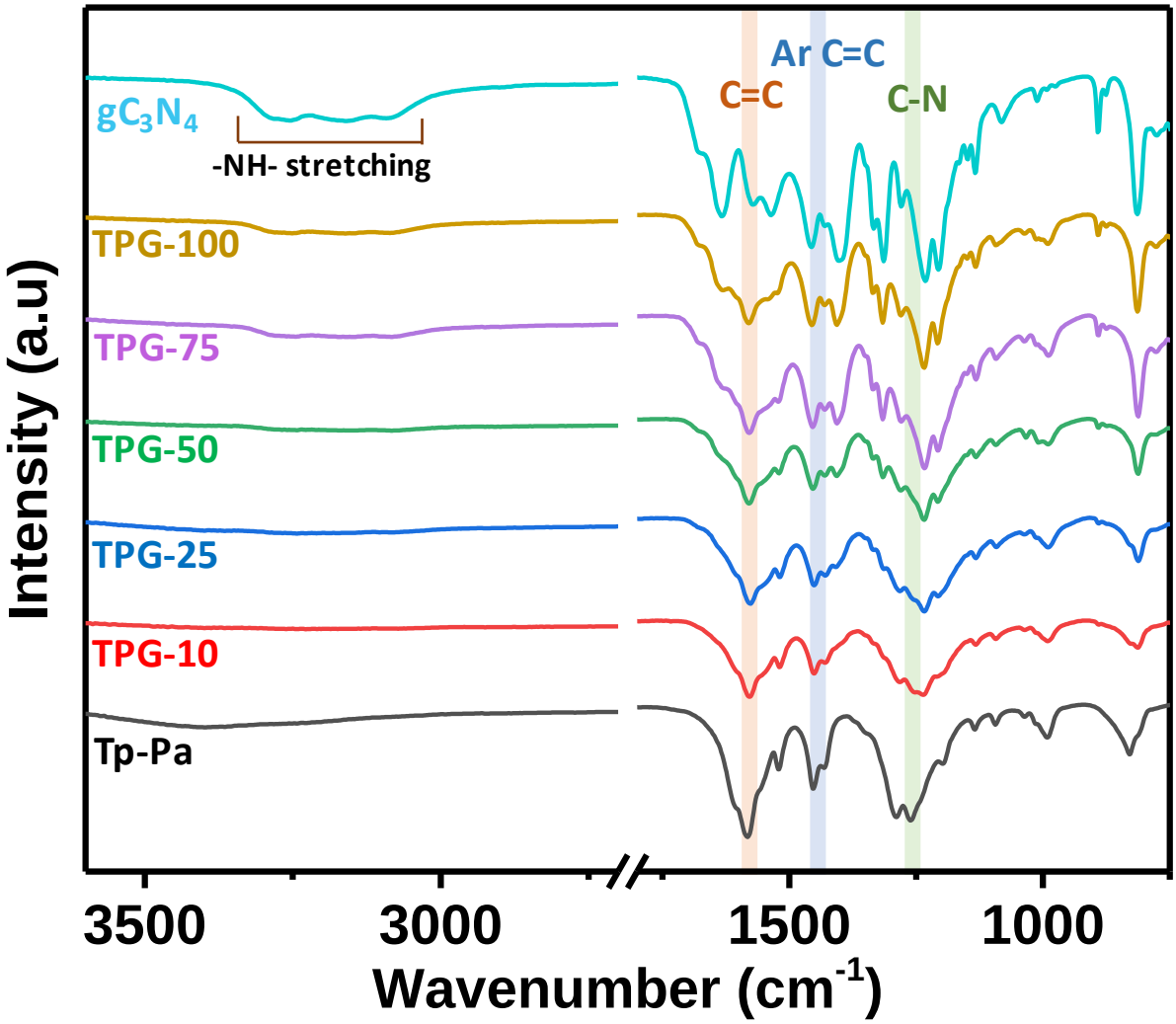

Figure S1. FT-IR spectrum of **Tp-Pa**, **gC_3N_4** and **TPG-75**.

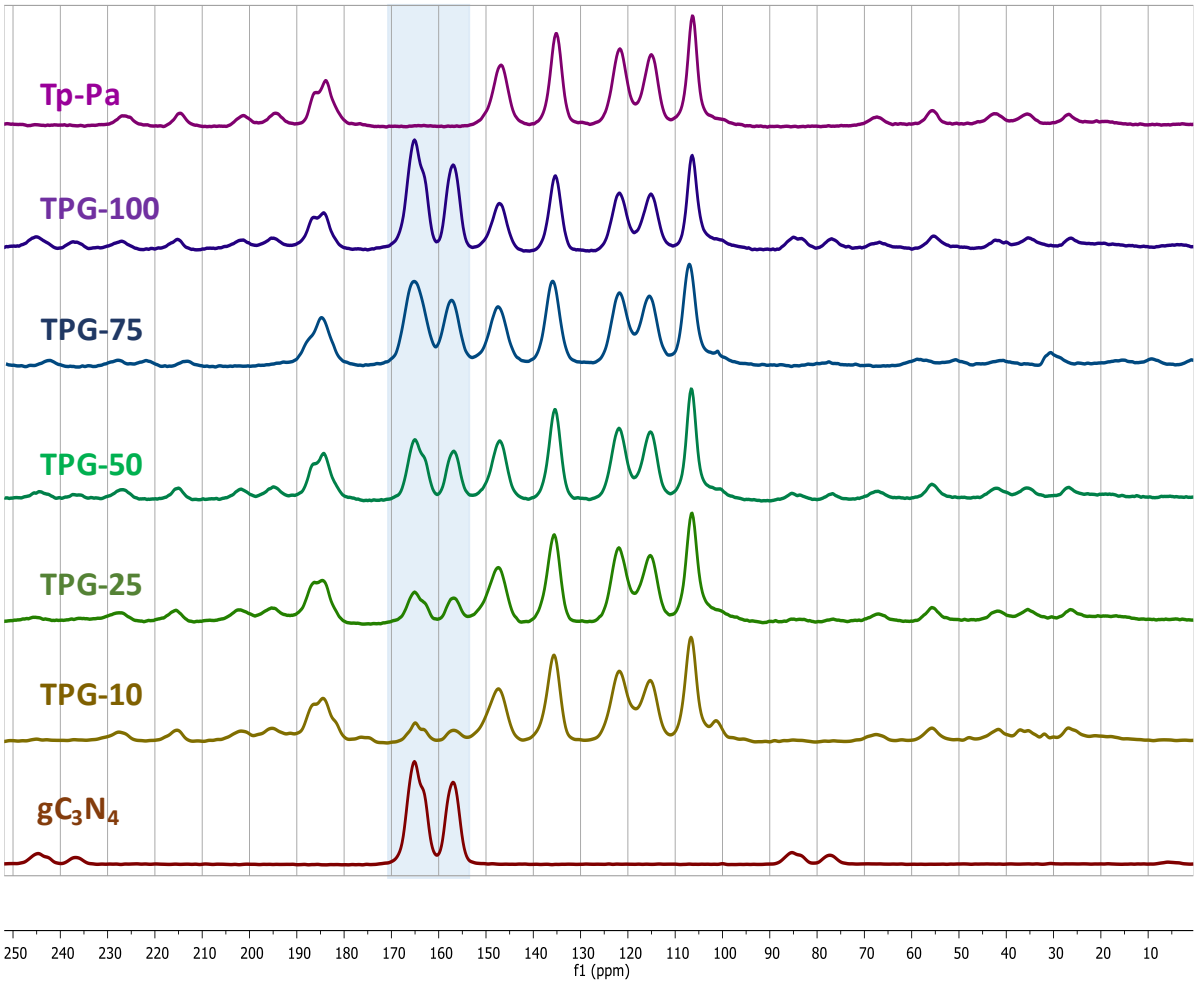

Figure S2. Solid state ^{13}C CP MAS spectra of **Tp-Pa**, **gC_3N_4**, and **TPG**s.

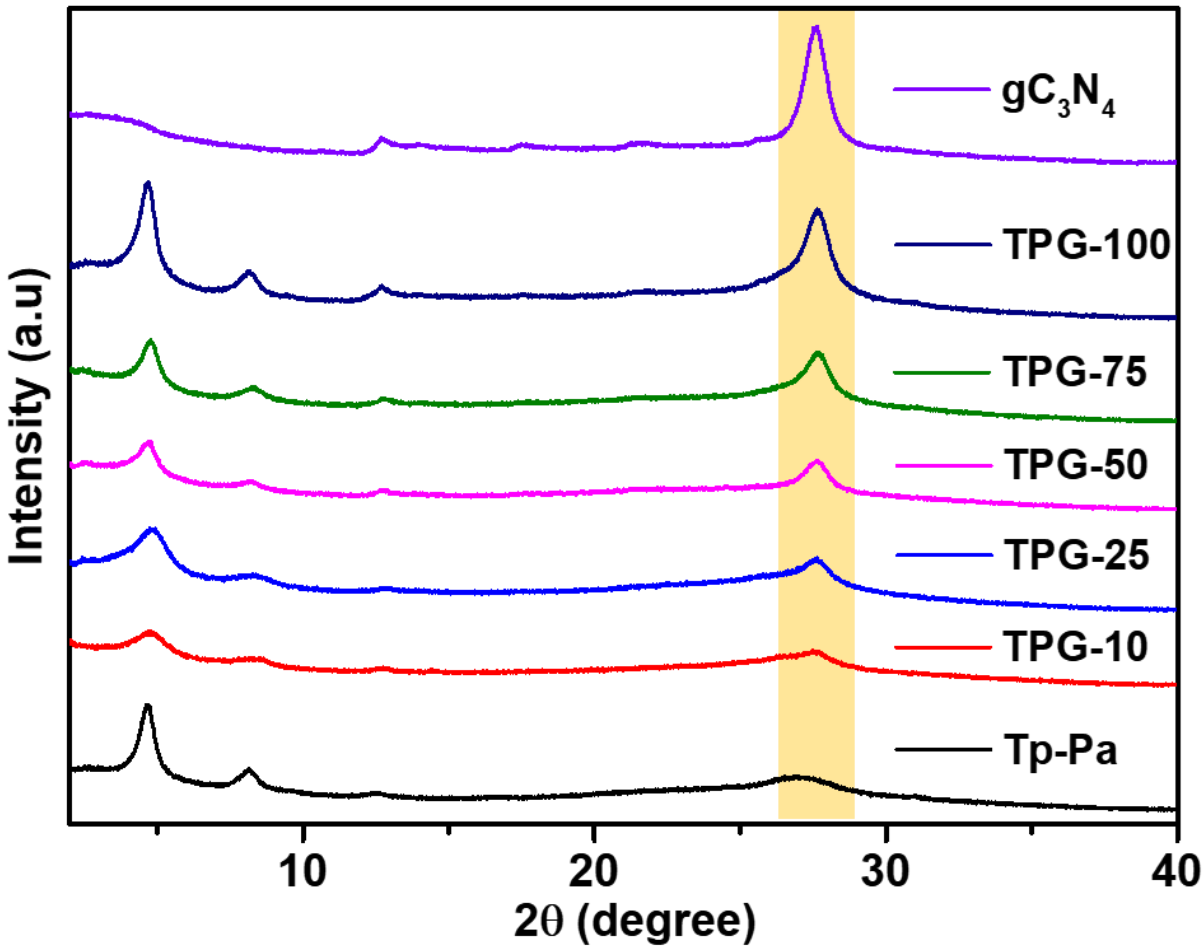

Figure S3. PXRD pattern of **Tp-Pa**, **gC_3N_4** and **TPG**s.

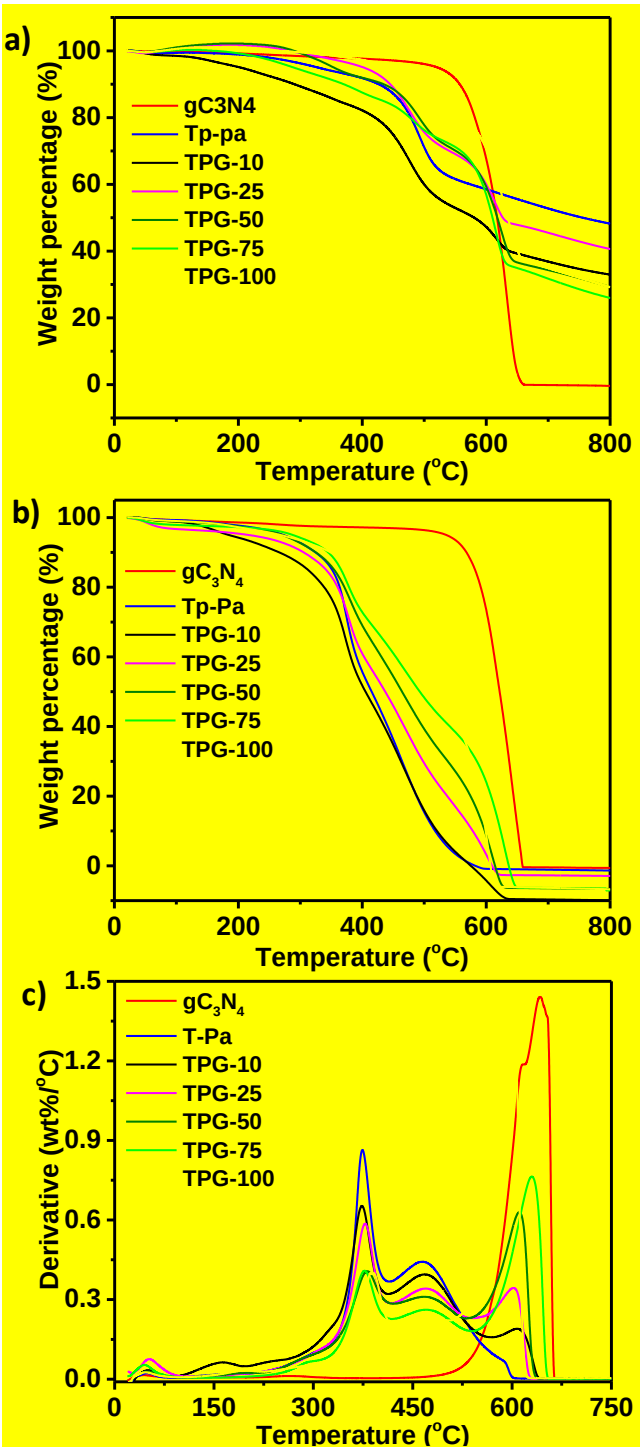

Figure S4. Thermogravimetric analysis of **Tp-Pa**, **gC_3N_4** and **TPG**s, a) under N_2, b) under air along with the corresponding c) DTA curve.

*The decomposition of all samples in the presence of air was also studied. It has been found that increasing the amount of **gC_3N_4** in TPGs increases the degradation temperature. The DTA curve shows two decomposition points, one for **Tp-Pa** occurring after 400 °C, and another one at around 600 °C for **gC_3N_4**. From the DTA curve, the percentage of **gC_3N_4** relative to **Tp-Pa** in the **TPG-x** was calculated and found to be 12.96%, 26.09%, 51.89%, 80.98%, and 106% for **TPG-10**, **TPG-25**, **TPG-50**, **TPG-75**, and **TPG-100**, respectively. The discrepancy in amount of gC3N4 might be due to the amount of sample used for analysing TGA.*

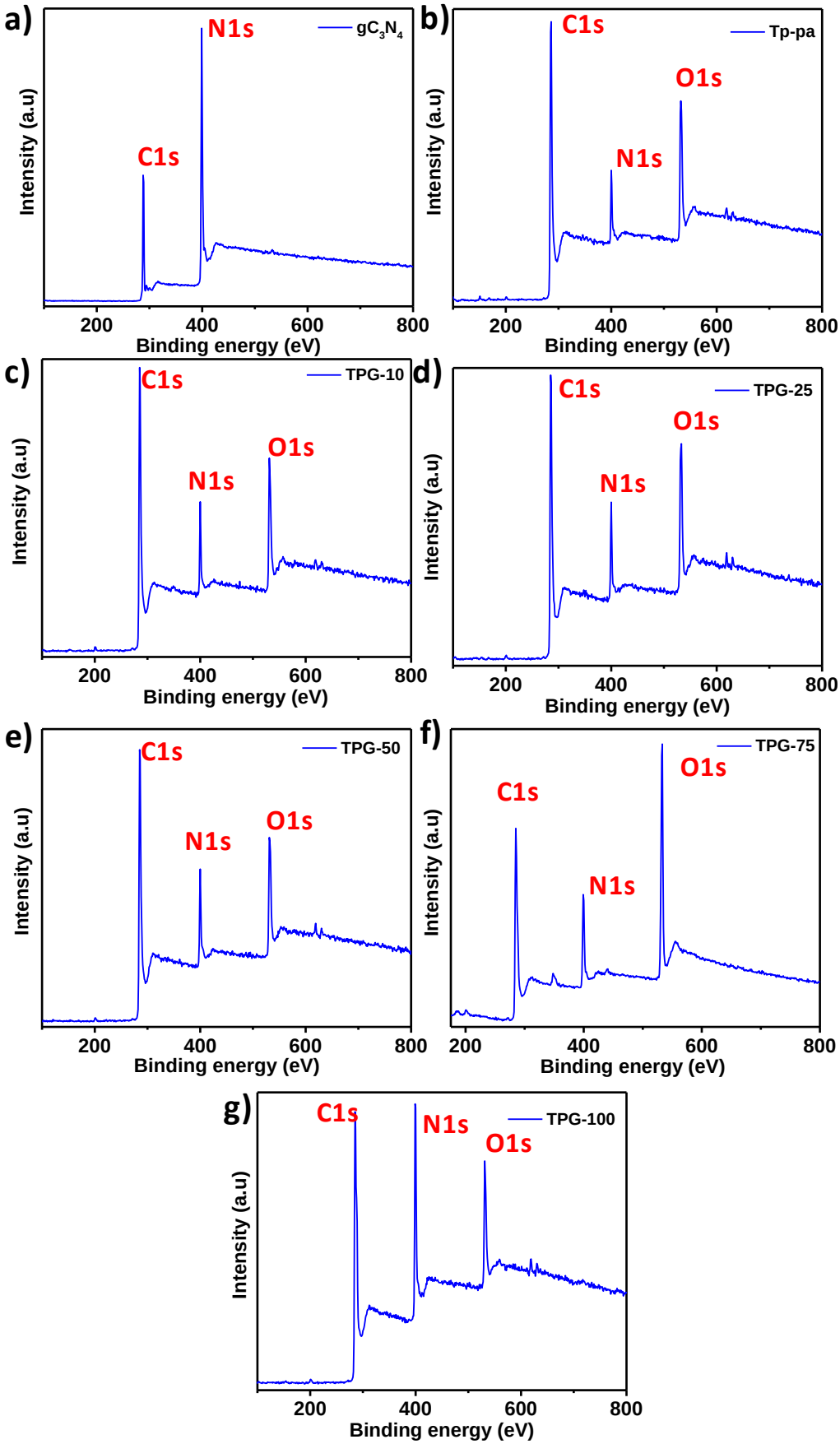

Figure S5. XPS survey scan spectra of a) **gC$_3$N$_4$**, b) **Tp-Pa**, c) **TPG-10**, d) **TPG-25**, e) **TPG-50**, f) **TPG-75**, g) **TPG-100**.

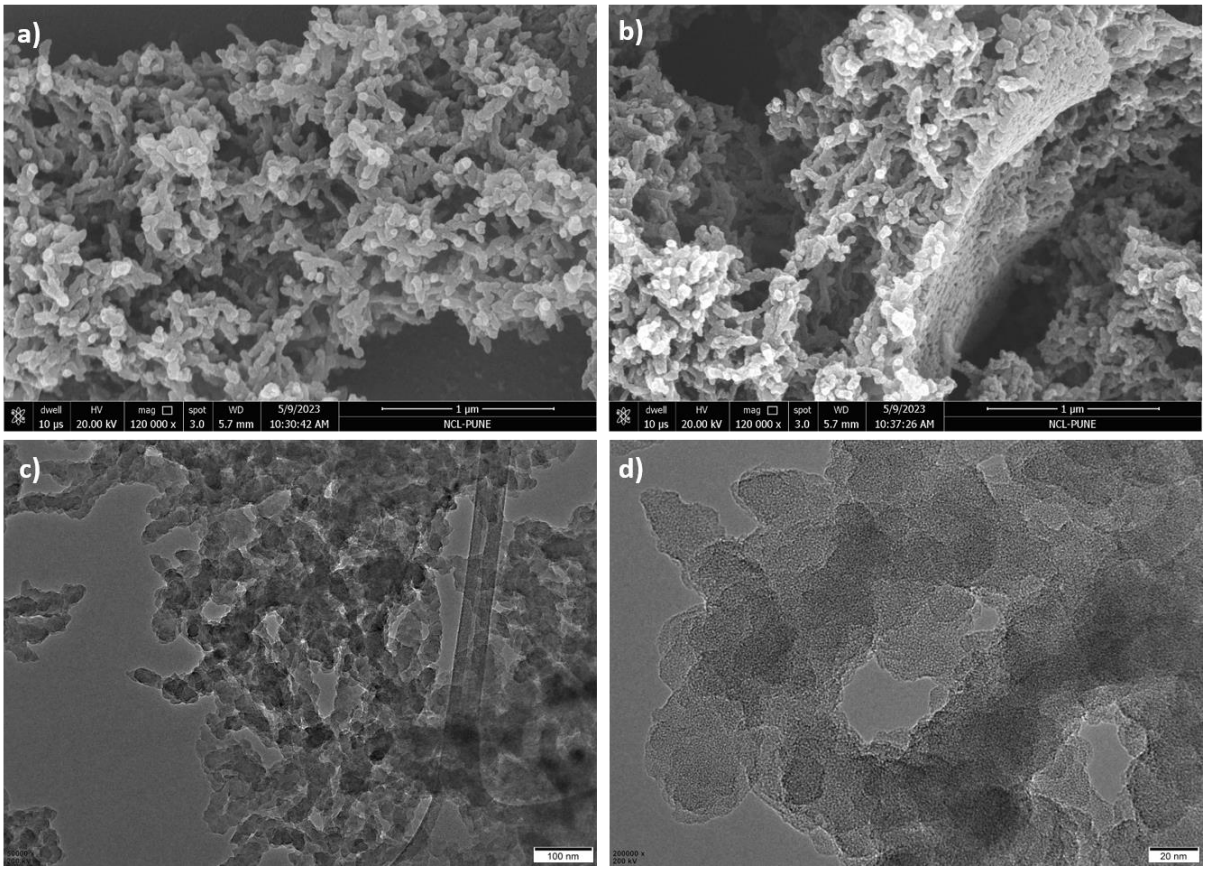

Figure S6. a, b) FE-SEM and c, d) HR-TEM images of **Tp-Pa**.

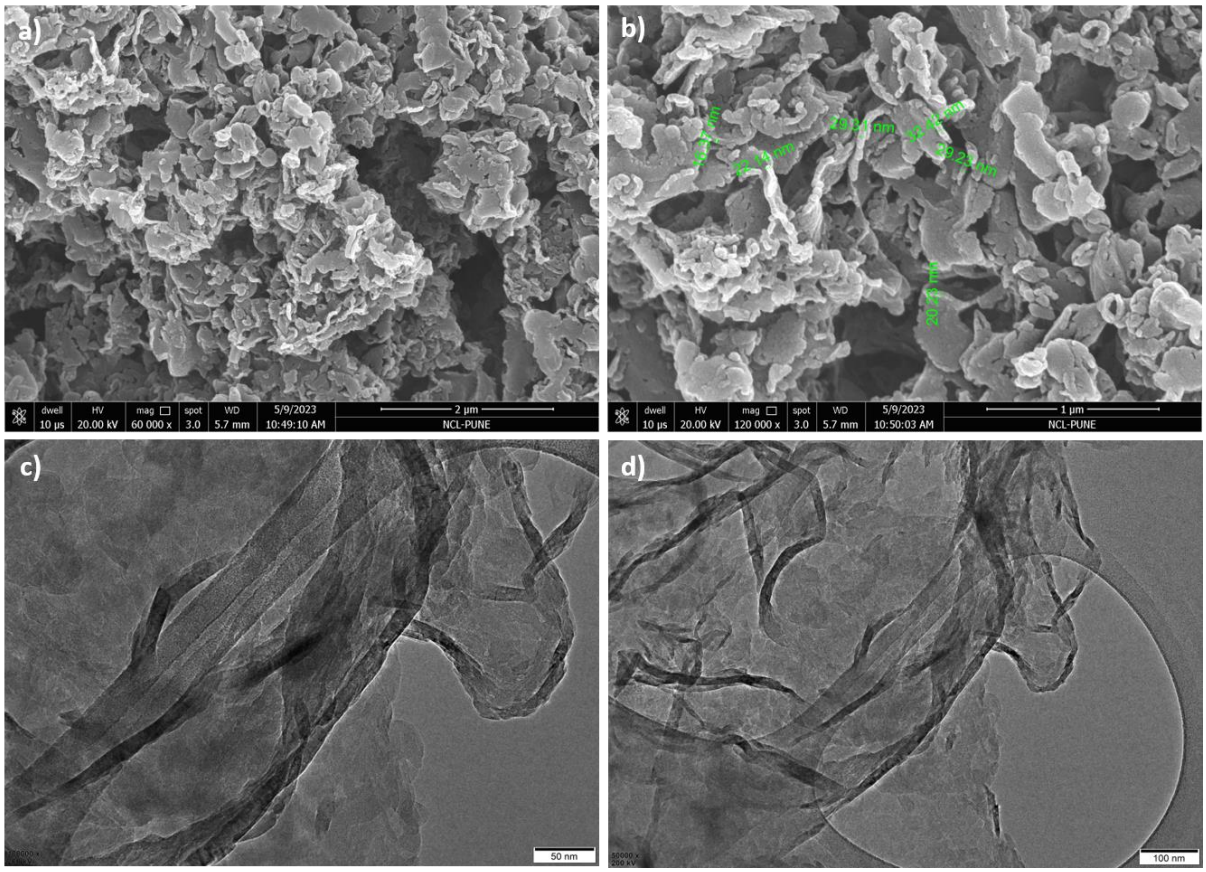

Figure S7. a, b) FE-SEM and c, d) HR-TEM images of **gC_3N_4.**

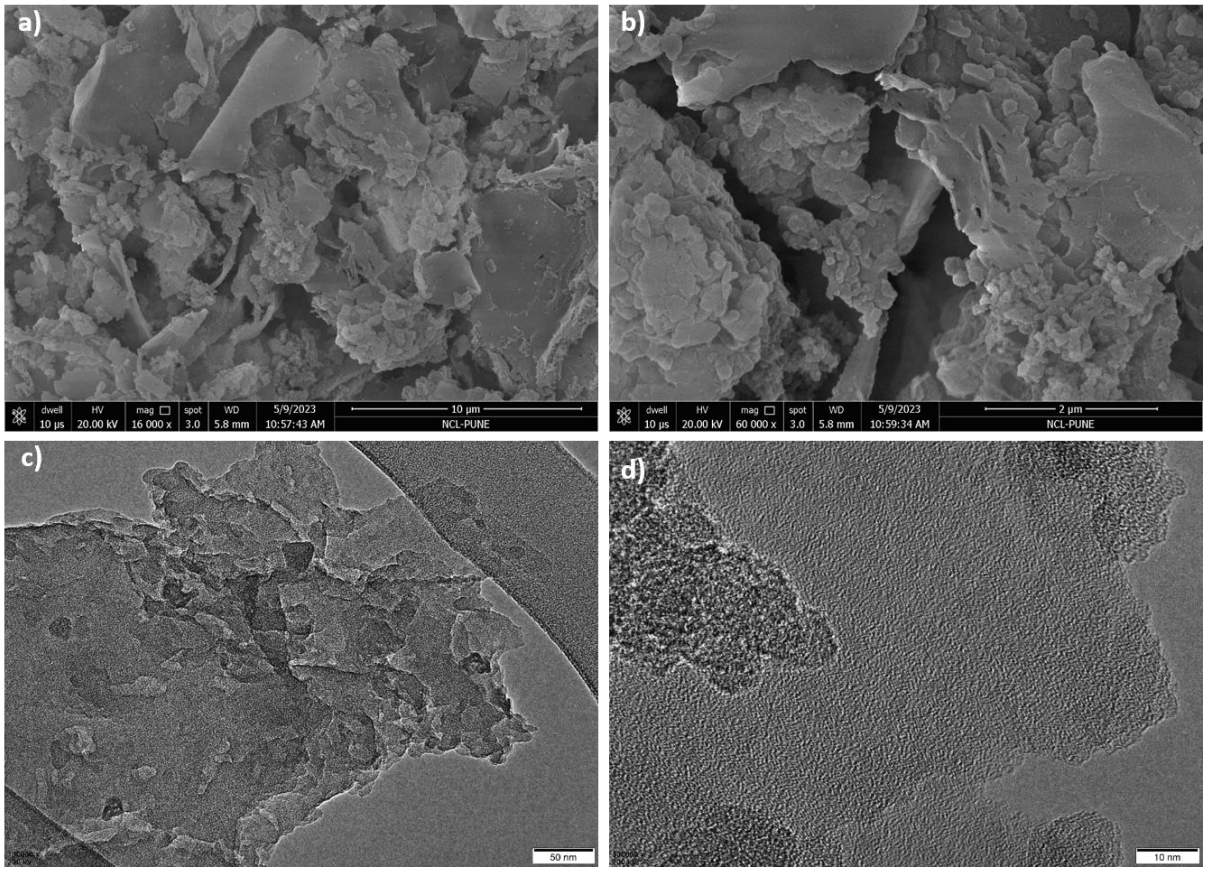

Figure S8. a, b) FE-SEM and c, d) HR-TEM images of **TPG-10**.

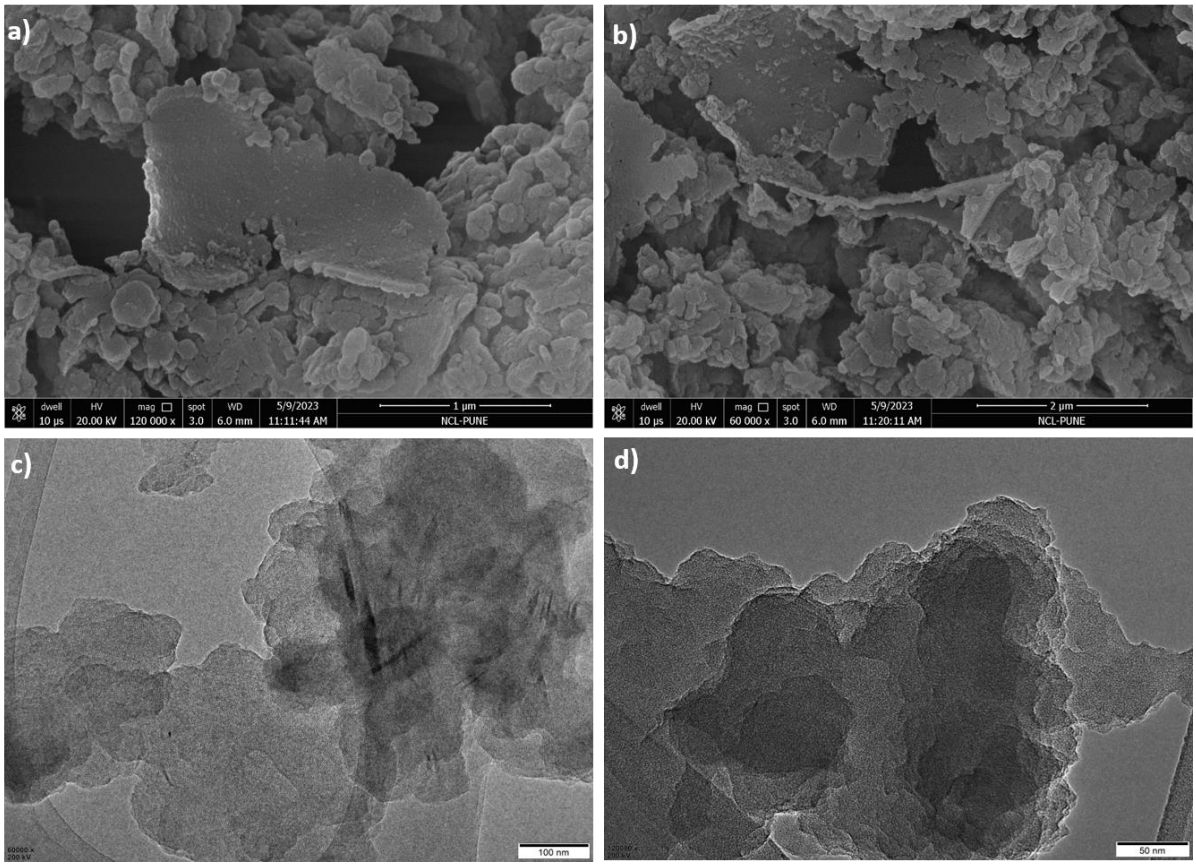

Figure S9. a, b) FE-SEM and c, d) HR-TEM images of **TPG-25**.

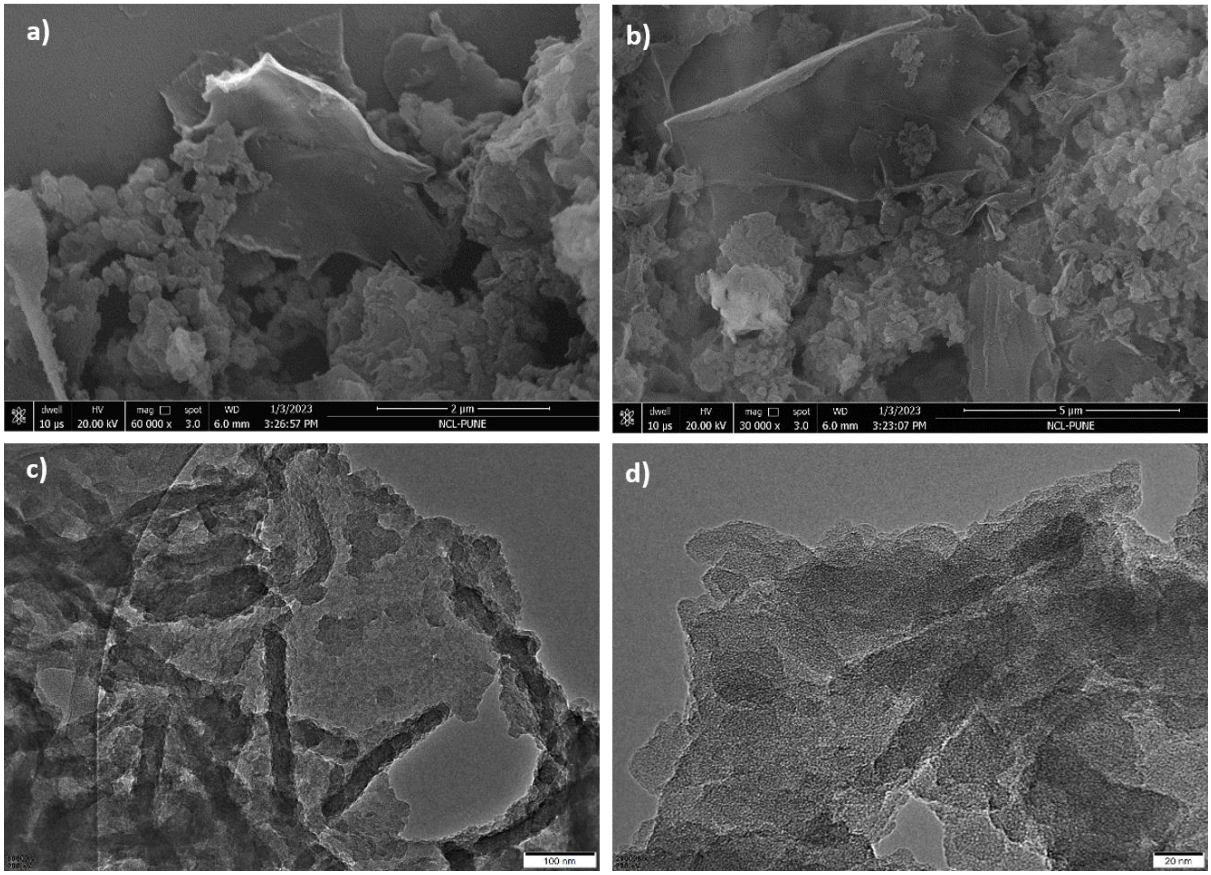

Figure S10. a, b) FE-SEM and c, d) HR-TEM images of **TPG-50**.

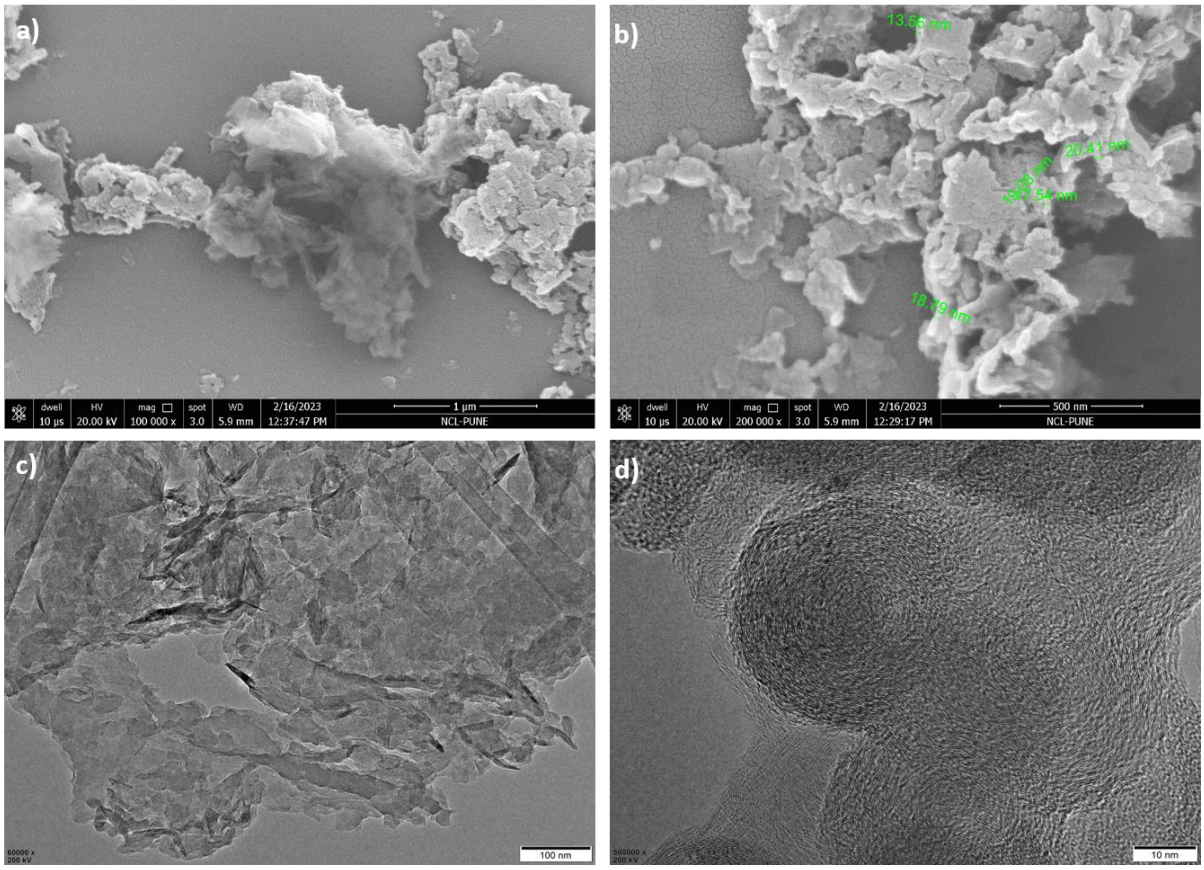

Figure S11. a, b) FE-SEM and c, d) HR-TEM images of **TPG-75**.

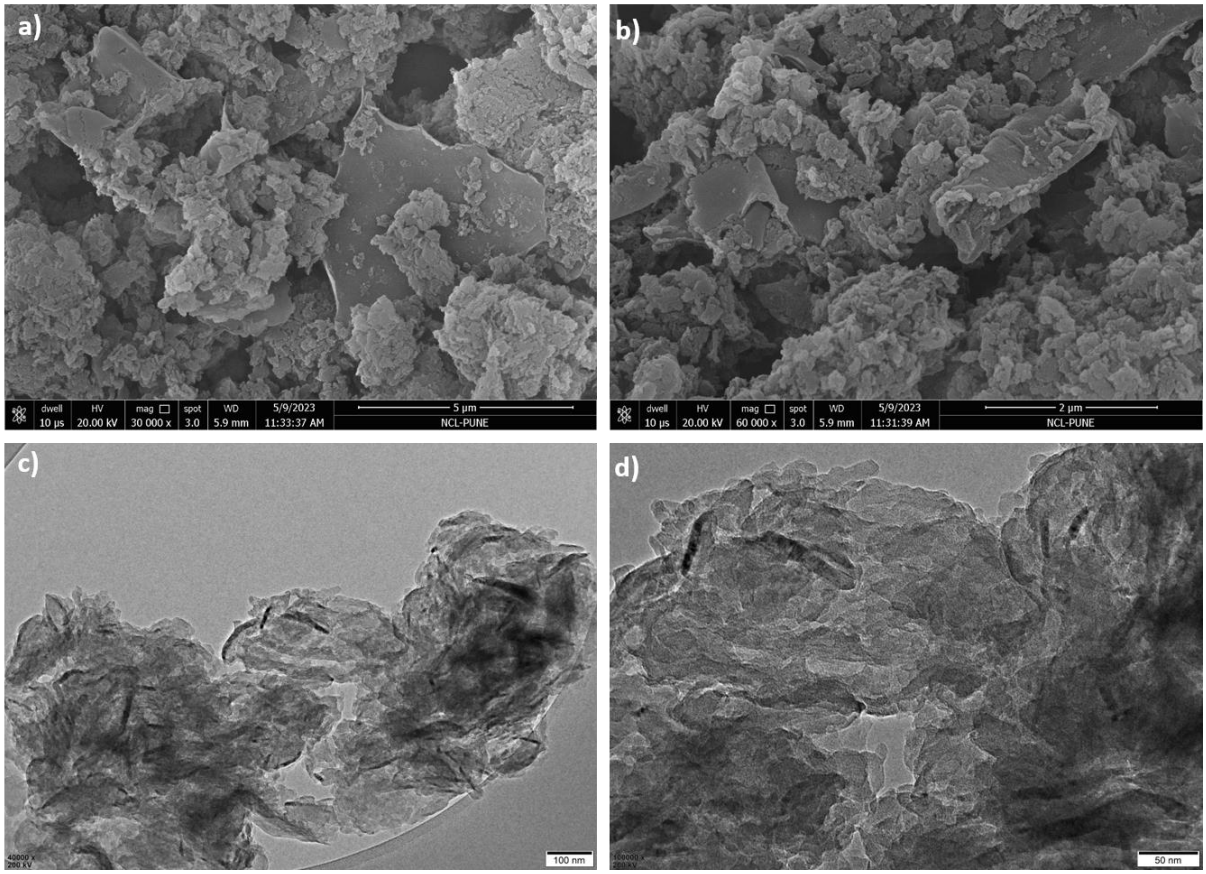

Figure S12. a, b) FE-SEM and c, d) HR-TEM images of **TPG-100**.

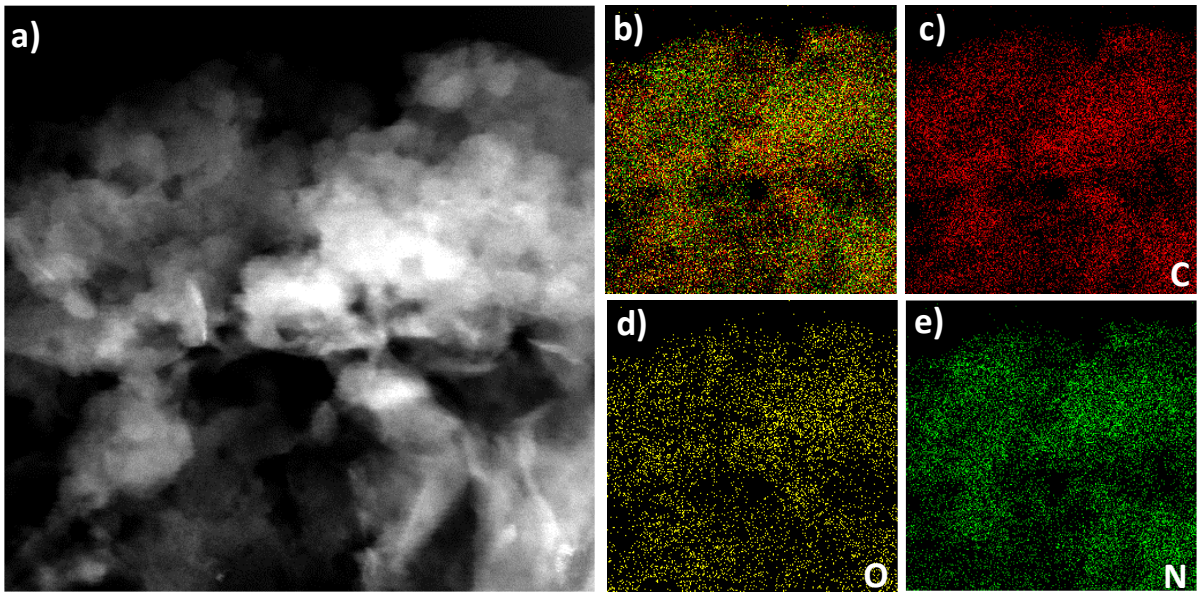

Figure S13. a) STEM image and elemental mapping of **TPG-75** showing b) overlay, c) C, d) O, and e) N, respectively.

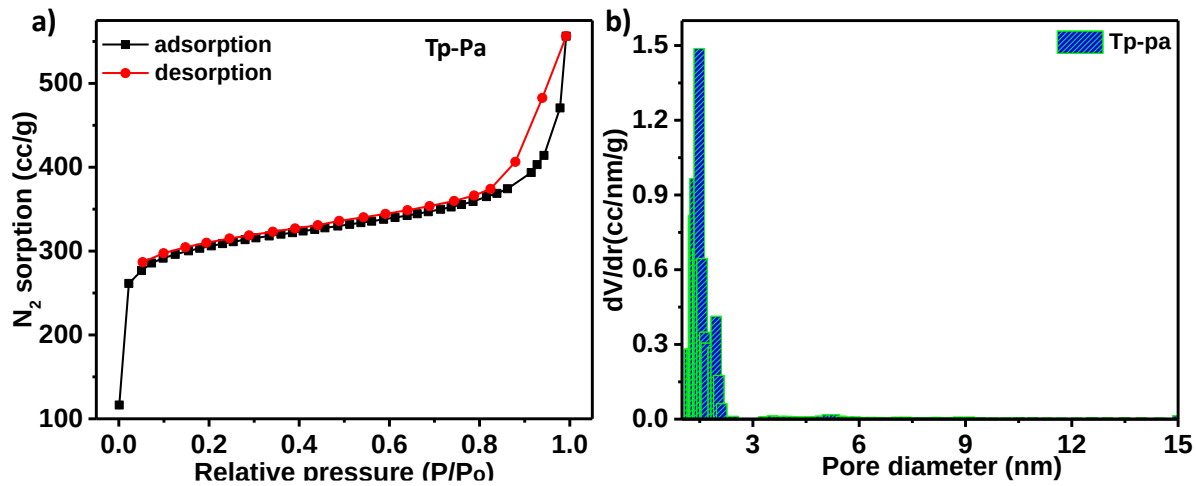

Figure S14. a) BET and b) pore size distribution of **Tp-Pa**.

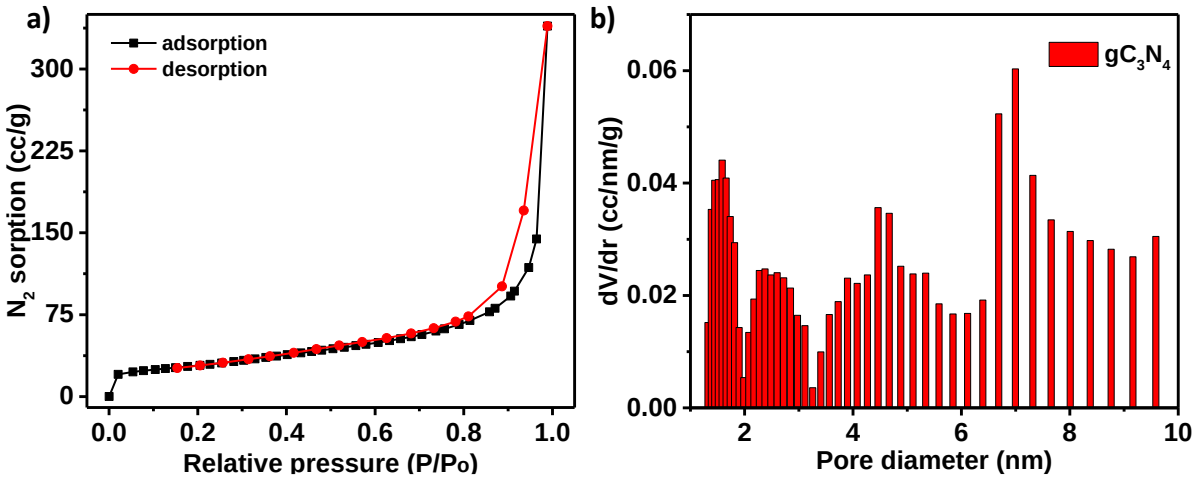

Figure S15. a) BET and b) pore size distribution of **gC_3N_4**.

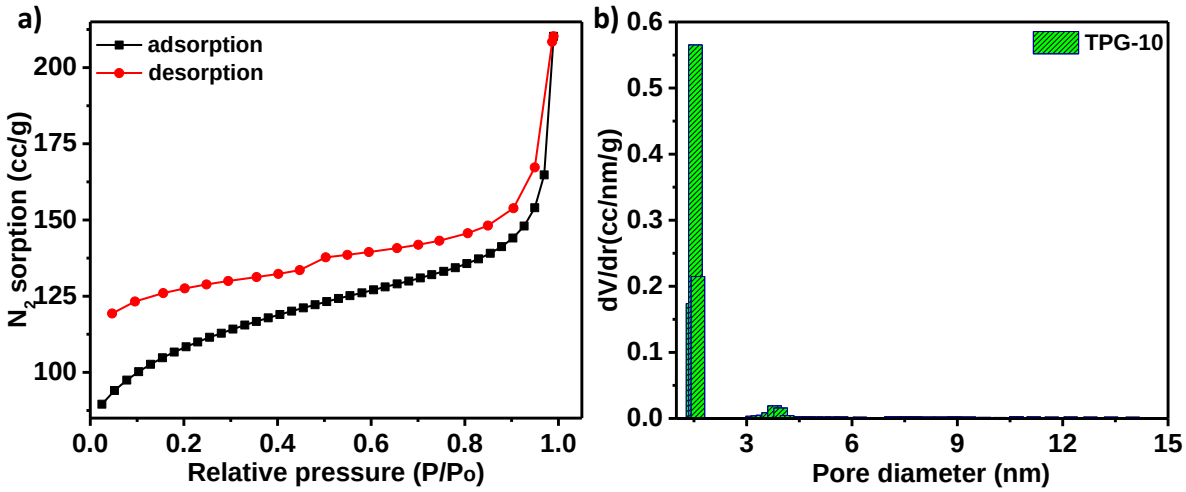

Figure S16. a) BET and b) pore size distribution of **TPG-10**.

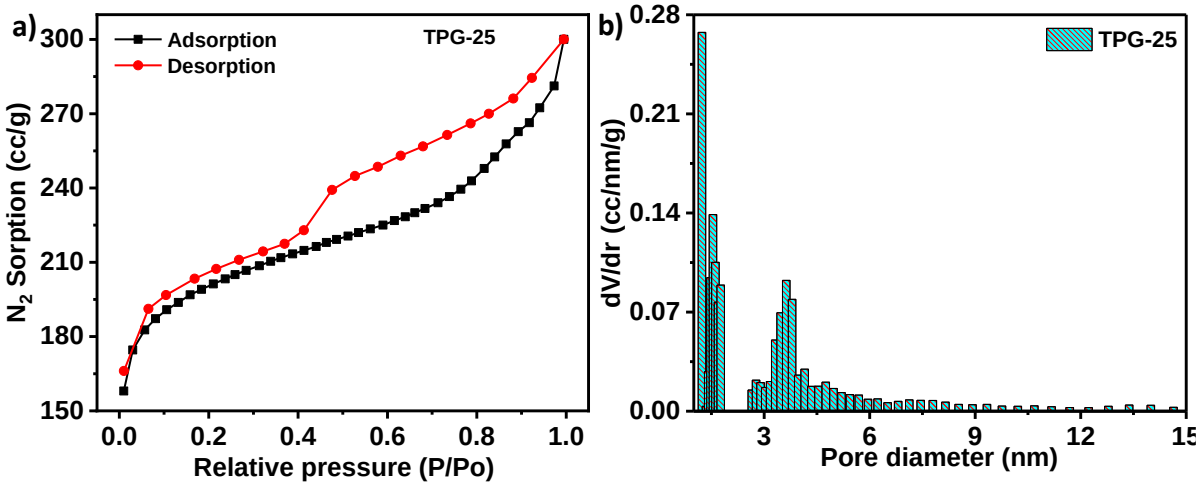

Figure S17. a) BET and b) pore size distribution of **TPG-25**.

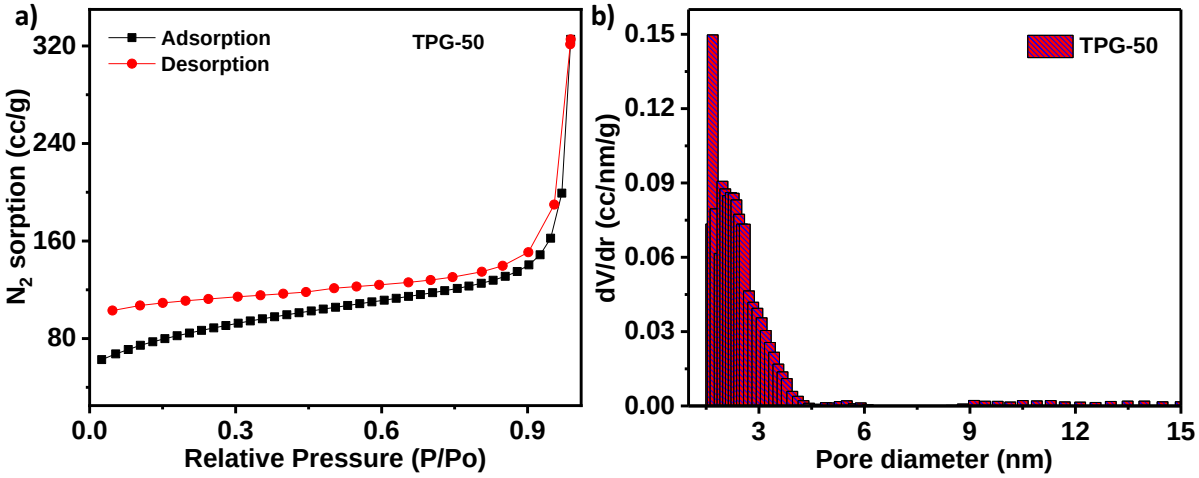

Figure S18. a) BET and b) pore size distribution of **TPG-50**.

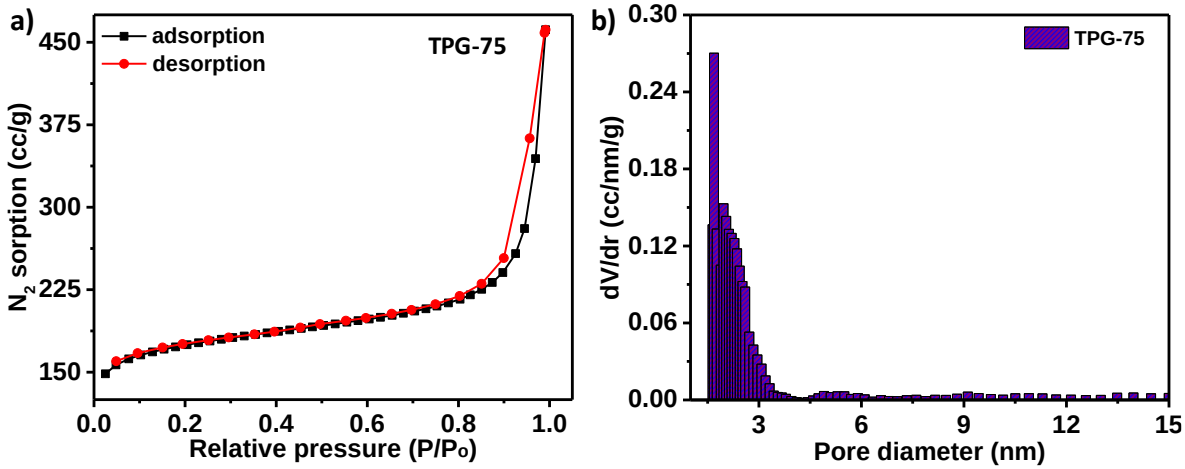

Figure S19. a) BET and b) pore size distribution of **TPG-75**.

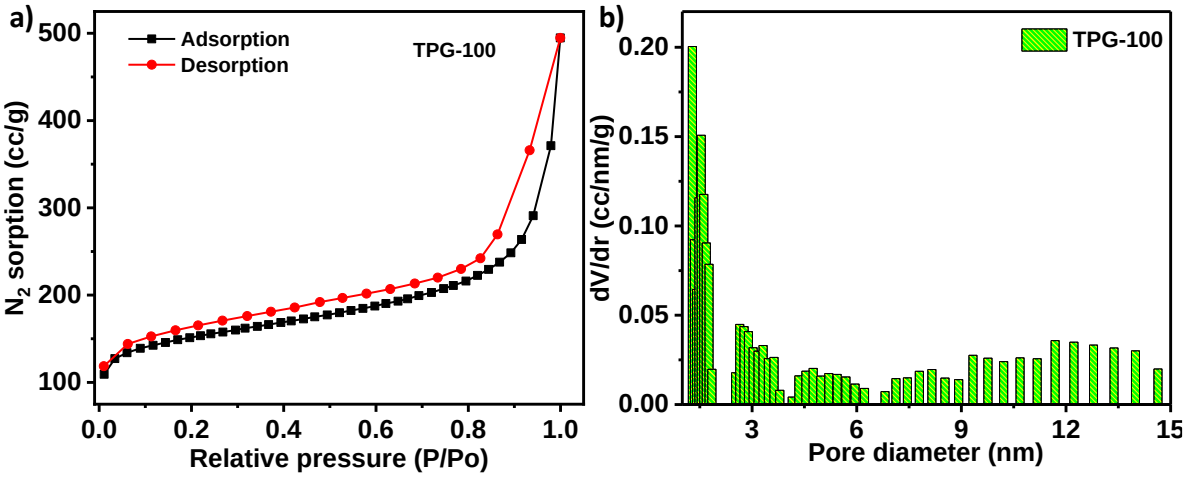

Figure S20. a) BET and b) pore size distribution of **TPG-100**.

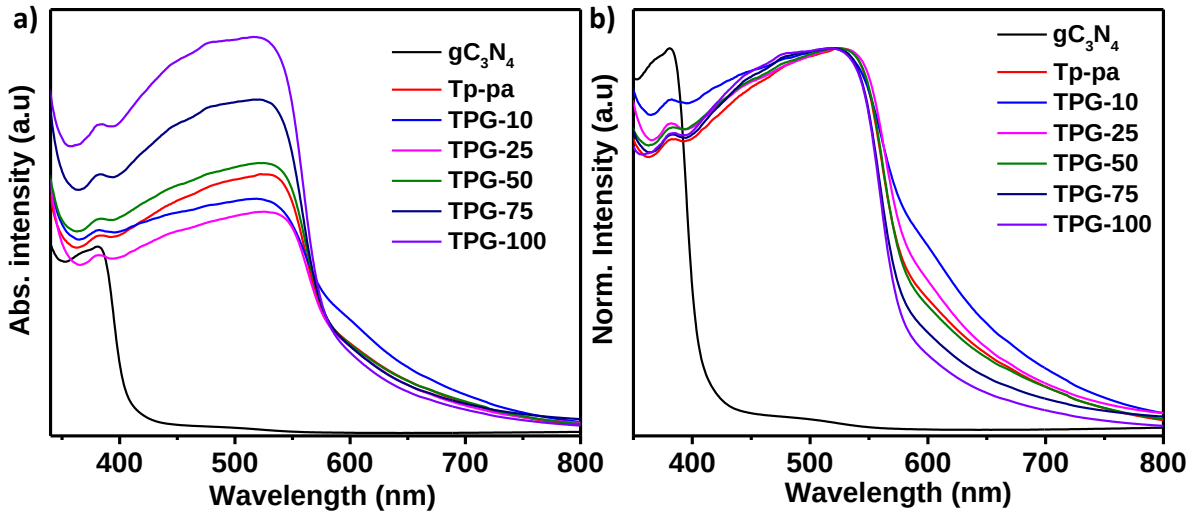

Figure S21. Solid-state UV-Vis DRS spectrum of **gC$_3$N$_4$**, **Tp-Pa**, and **TPGs**.

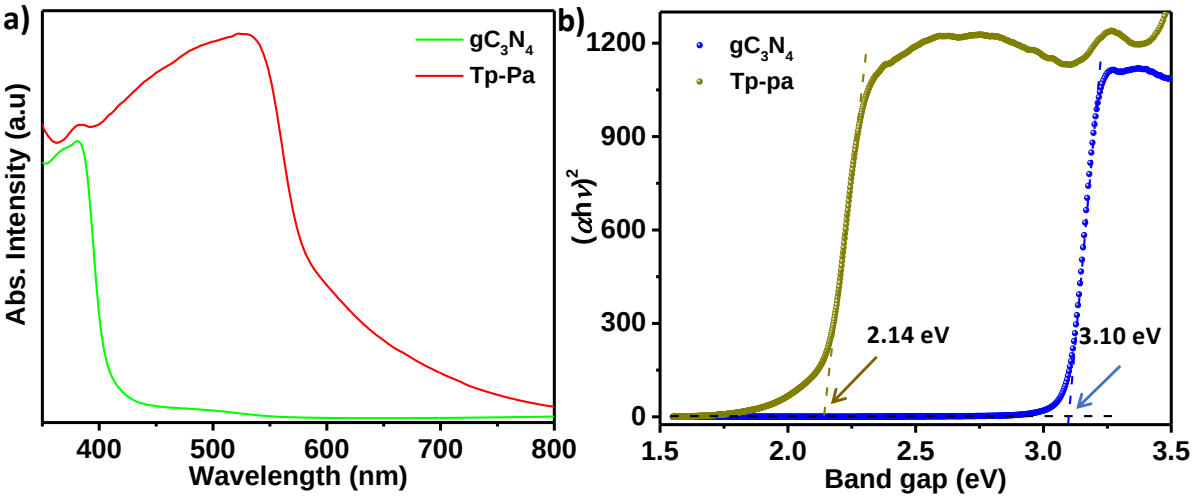

Figure S22. a) Solid-state UV-Vis DRS spectrum of **gC$_3$N$_4$** and **Tp-Pa**. b) corresponding tauc plot of **gC$_3$N$_4$** and **Tp-Pa**.

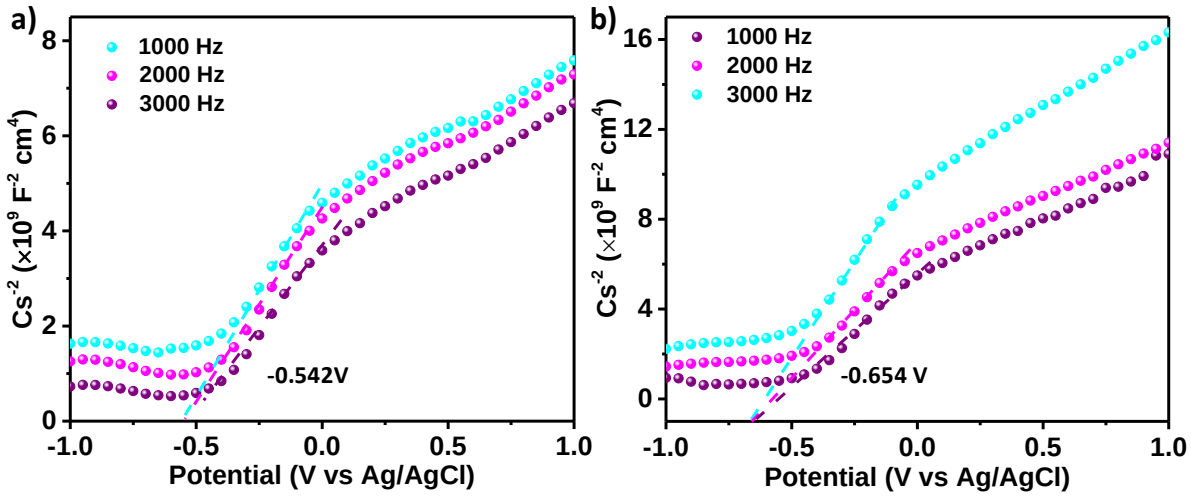

Figure S23. Mott-Schottky measurements with varying frequencies for a) **Tp-Pa**, b) **gC_3N_4**.

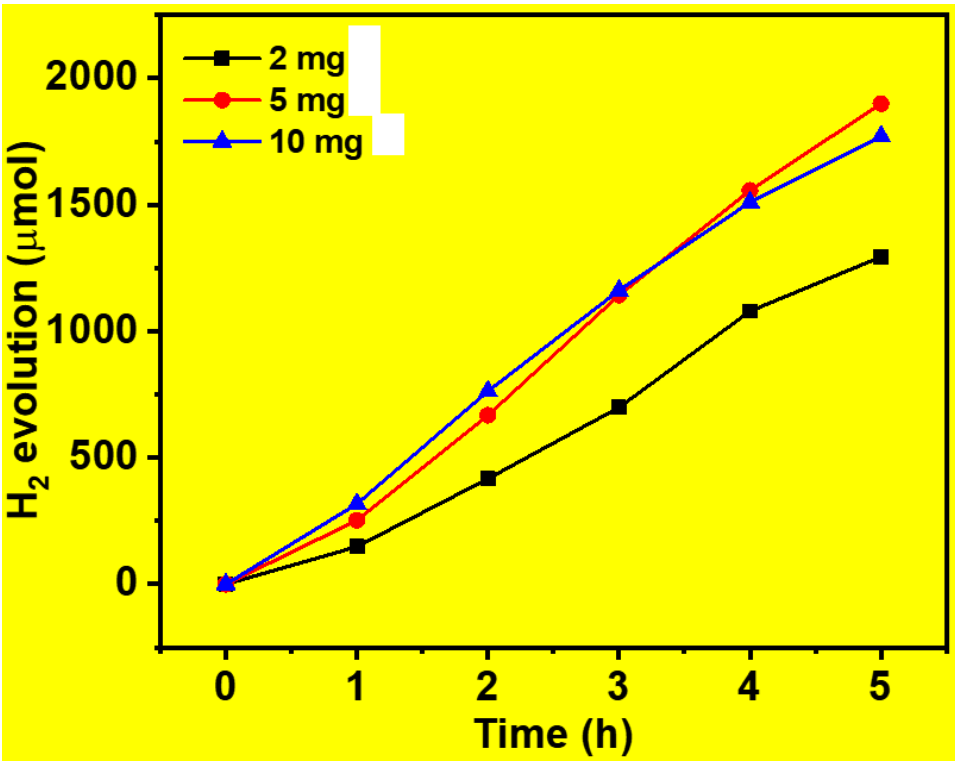

Figure S24. Comparison of the HER of **TPG-75** with varying catalyst amount.

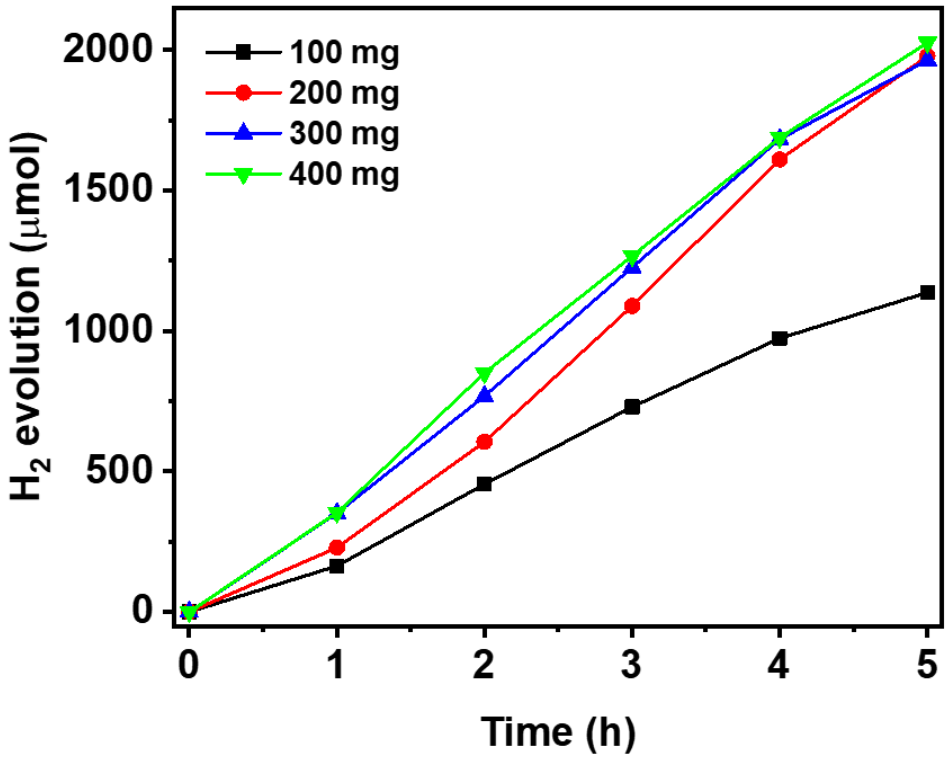

Figure S25. Comparison of the HER of **TPG-75** with varying SED amounts.

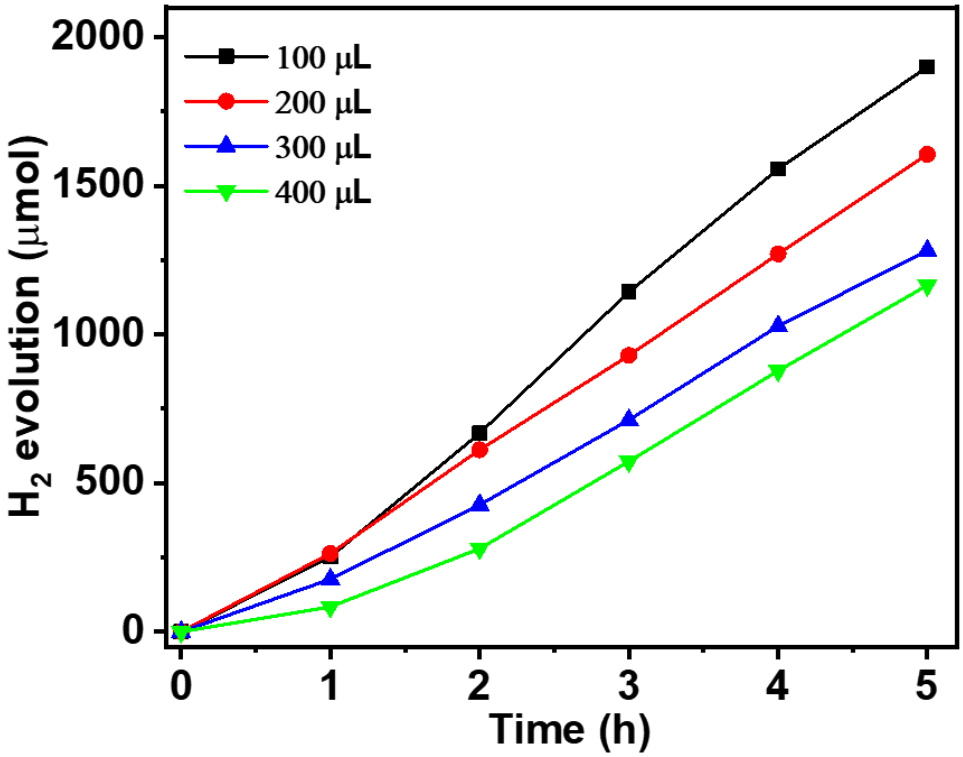

Figure S26. Comparison of the HER of **TPG-75** with varying amounts of co-catalyst.

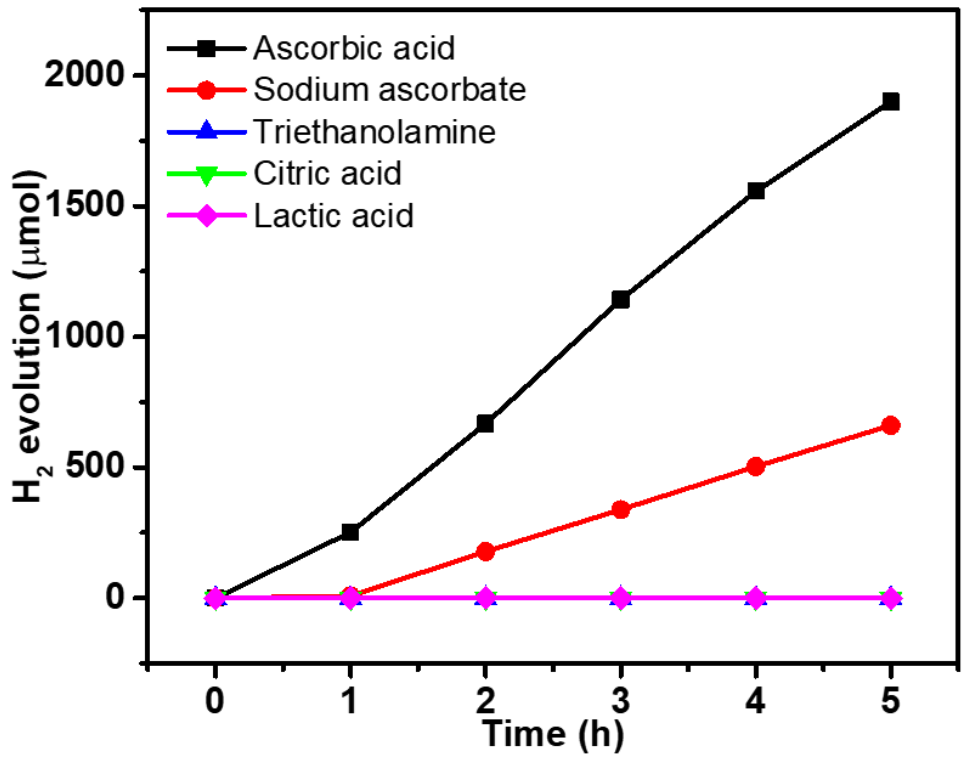

Figure S27. Comparison of the HER of **TPG-75** with varying SED.

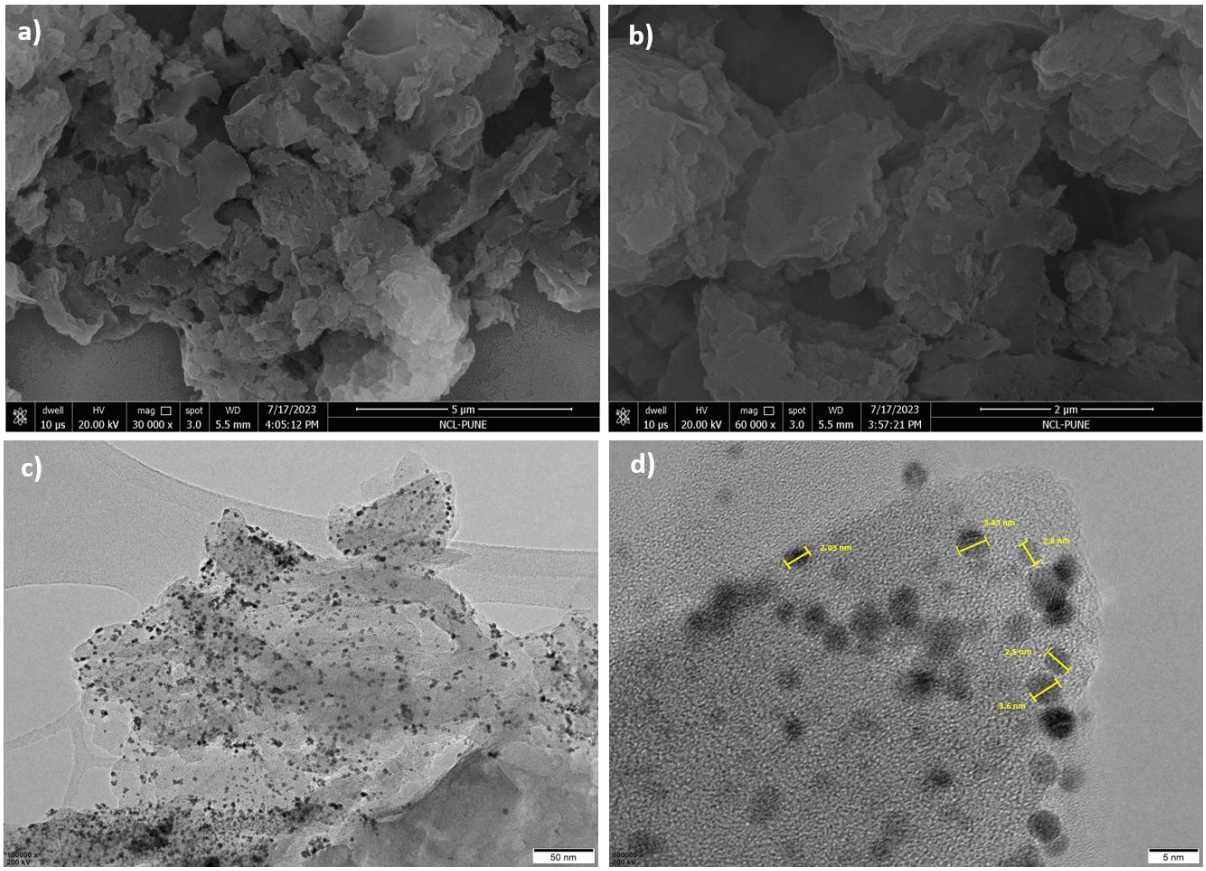

Figure S28. HR-TEM images of **TPG-75** after cyclic studies.

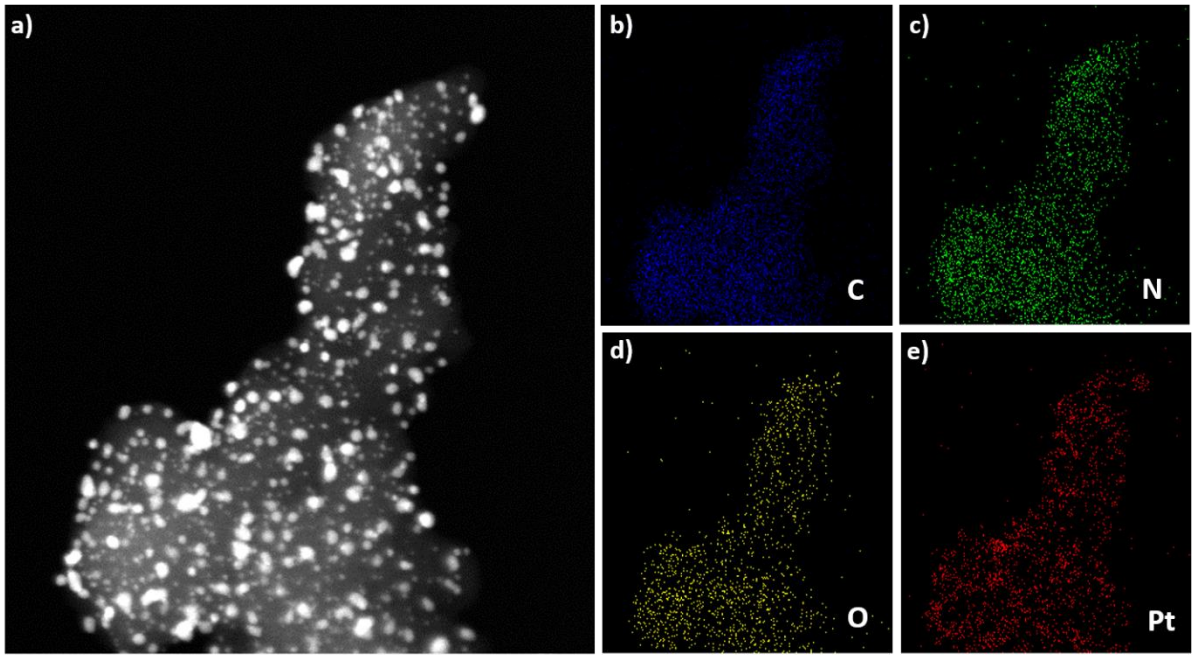

Figure S29. a) STEM image of **TPG-75** and elemental mapping of **TPG-75** showing b) C, c) N, d) O, and e) Pt NPs, respectively.

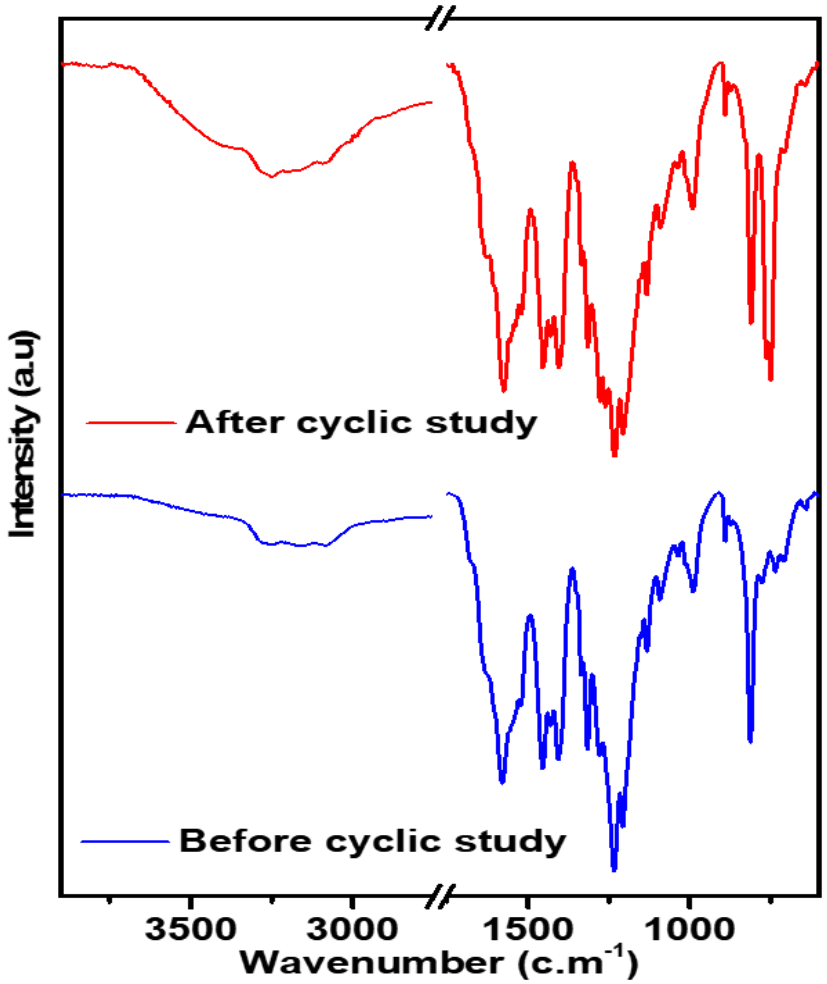

Figure S30. FT-IR spectra of **TPG-75** before and after cyclic studies.

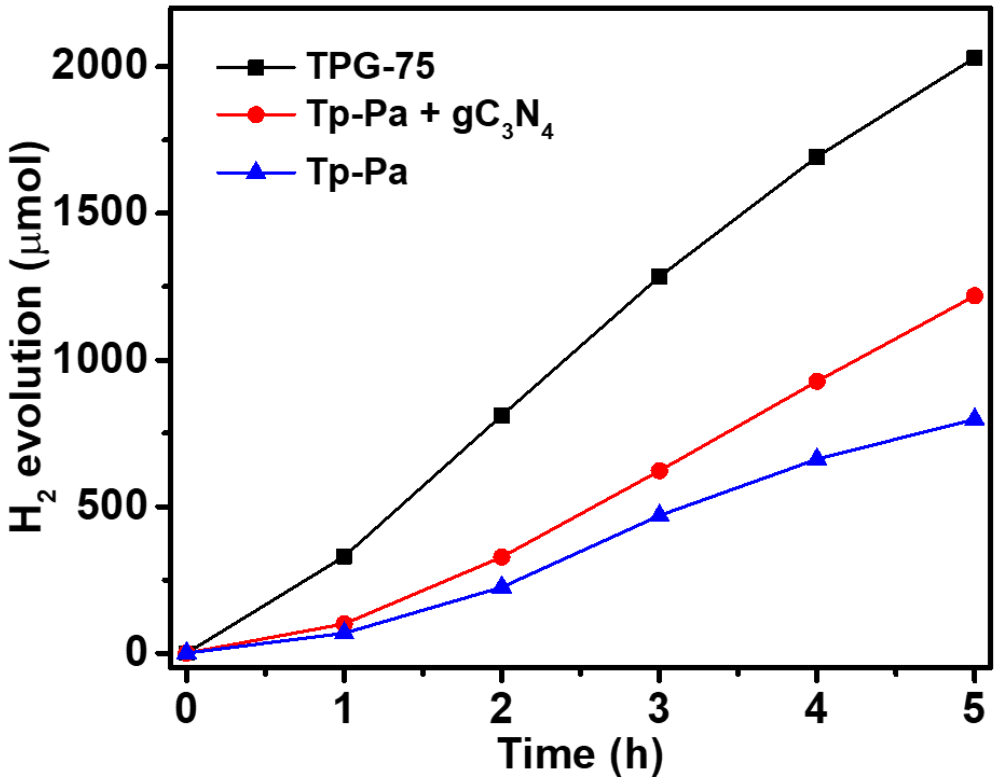

Figure S31. Effect of physical mixing of **Tp-Pa** and **gC_3N_4** on HER. Comparison of the HER of **Tp-Pa**, physical mixing of **Tp-Pa** with **gC_3N_4** and **TPG-75**.

a)

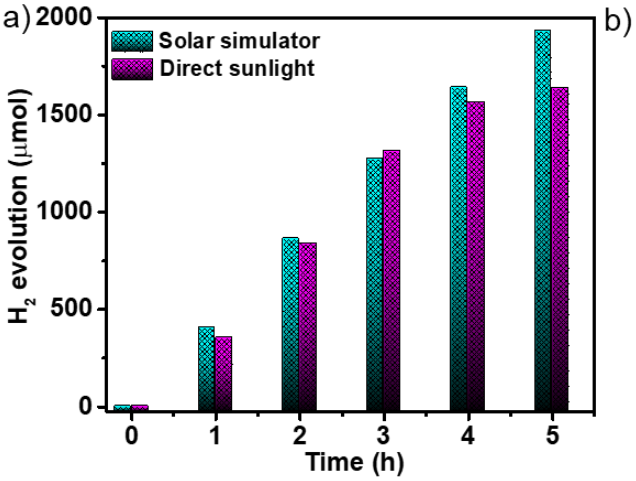

b)

Time (h)	Average sunlight intensity (mW/cm^2)
1	144
2	171
3	165
4	155
5	125

Figure S32. a) Comparison of the HER performance of **TPG-75** under solar simulator and direct sunlight irradiation and b) the average sunlight intensity during 5 h HER experiment.

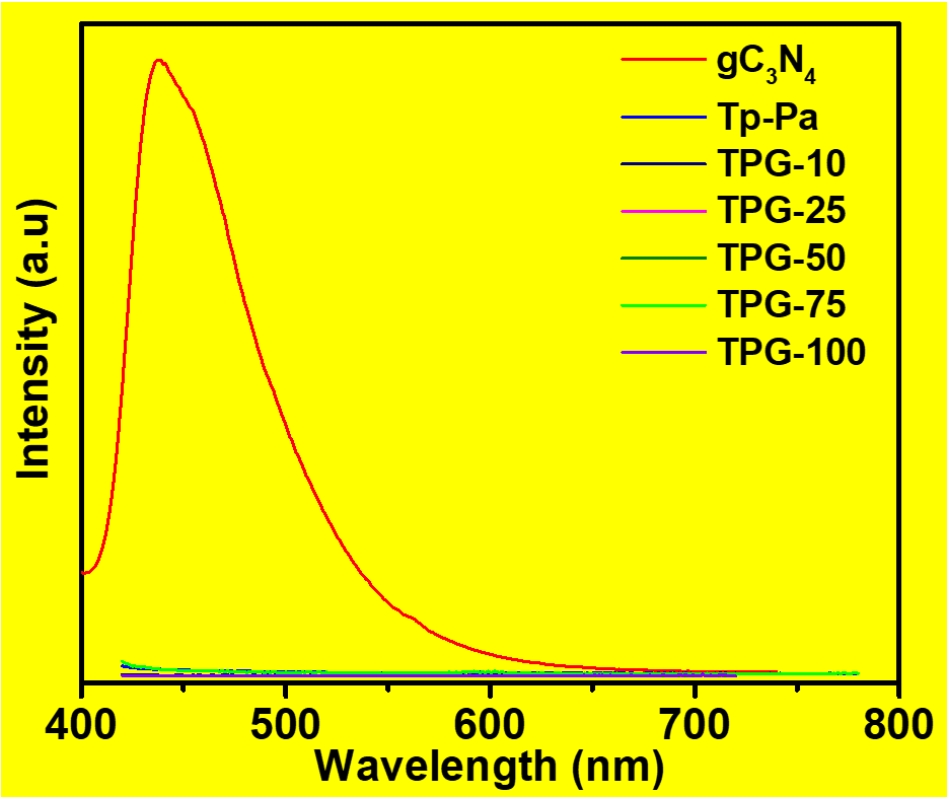

Figure S33. Photoluminescence spectra of **gC$_3$N$_4$**, **Tp-Pa** and **TPG-**x derivatives λ_{ex} for **gC$_3$N$_4$** is 370 nm and for **Tp-Pa**, **TPG-75** is 420 nm.

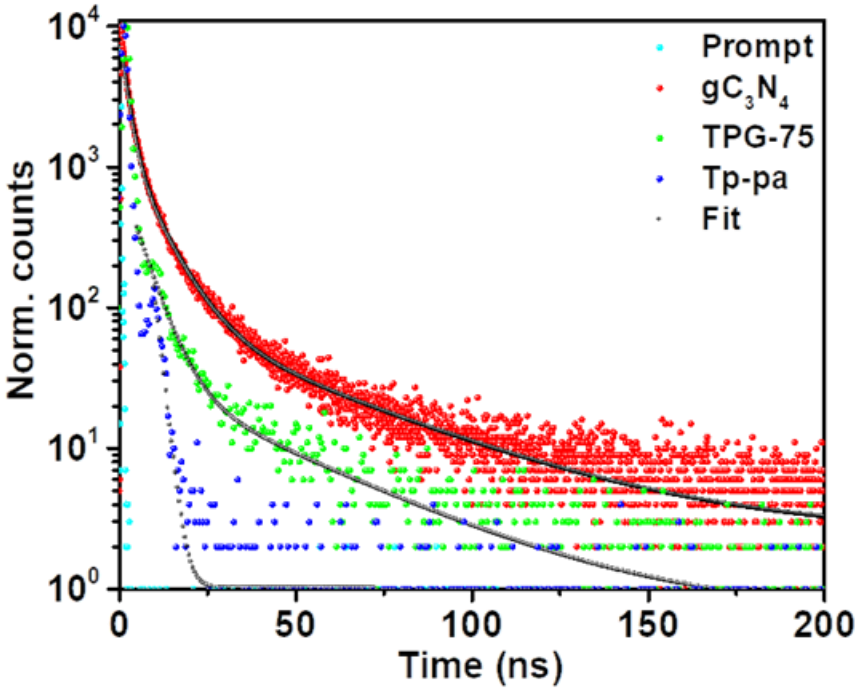

Figure S34. Photoluminescence lifetime spectra of emission of **gC$_3$N$_4$**, **TPG-75,** and **Tp-Pa** monitored at 445 nm, λ_{ex} = 345 nm.

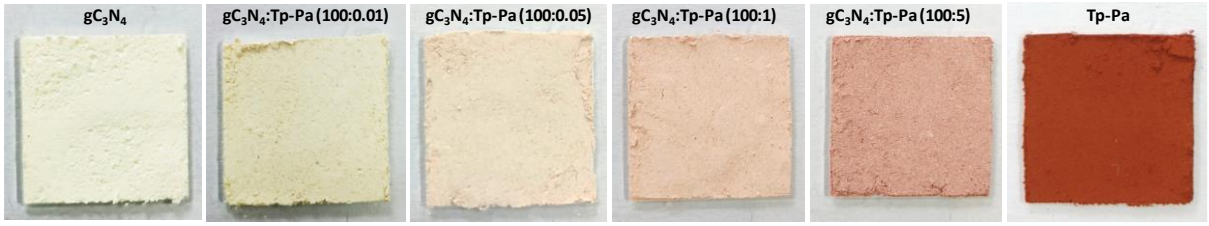

Figure S35. Photographs of pristine **gC$_3$N$_4$** and **gC$_3$N$_4$** mixed with **Tp-Pa** in different ratios.

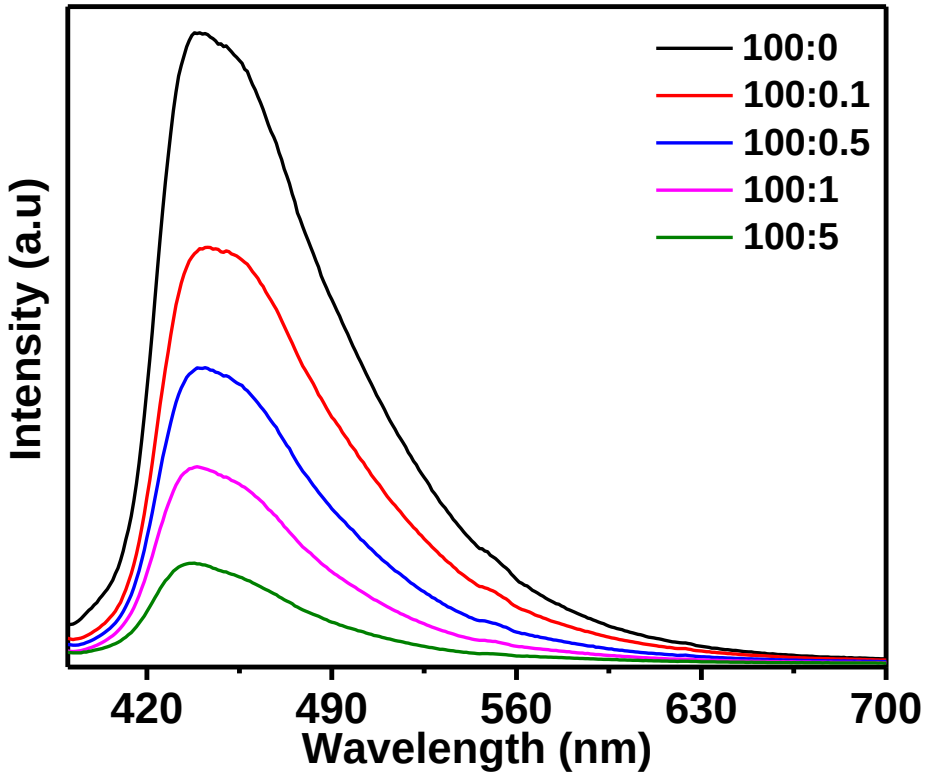

Figure S36. Photoluminescence emission of pristine **gC$_3$N$_4$** and **gC$_3$N$_4$** mixed with **Tp-Pa** in different ratios in the solid state (**gC$_3$N$_4$:Tp-Pa**), λ_{ex} = 370 nm.

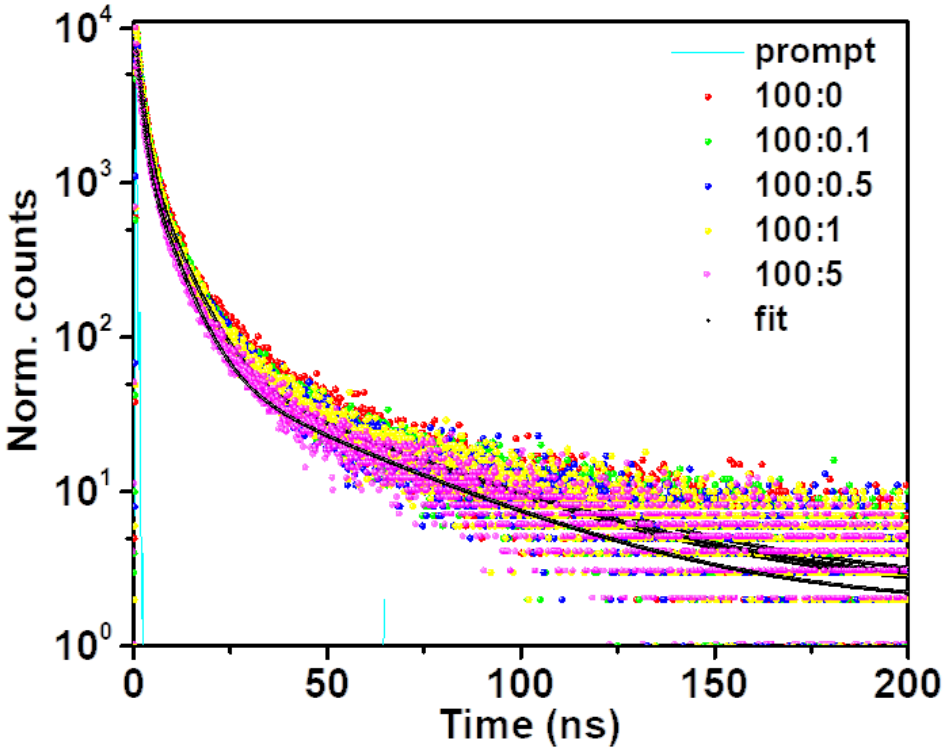

Figure S37. Photoluminescence lifetime spectra of pristine **gC_3N_4** and **gC_3N_4** mixed with **Tp-Pa** in different ratios (**gC_3N_4:Tp-Pa)**. λ_{ex} = 345 nm, λ_{mon} = 445 nm.

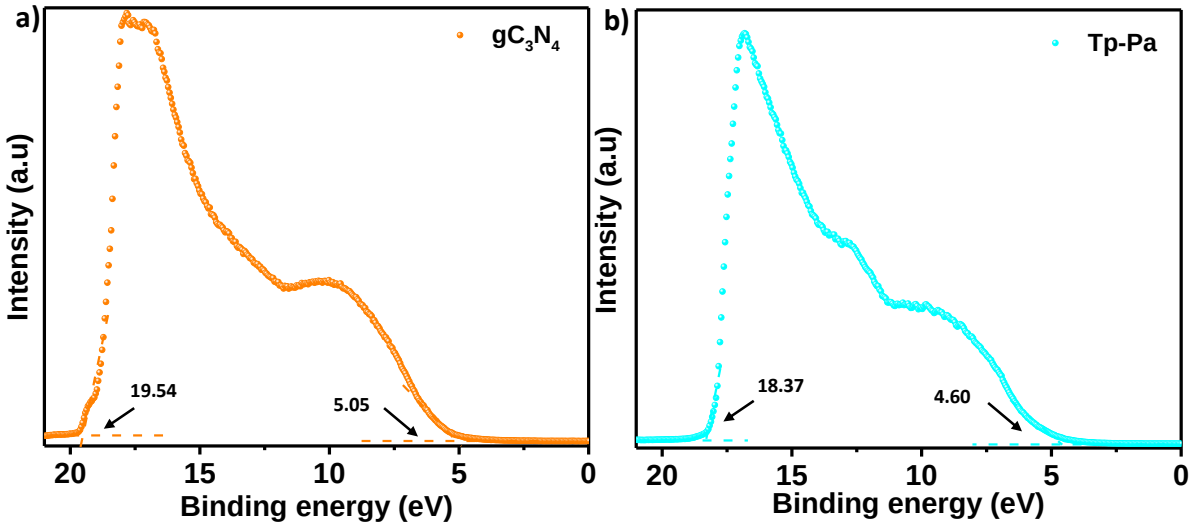

Figure 38. UPS spectrum of a) **gC_3N_4**, b) **Tp-Pa**.

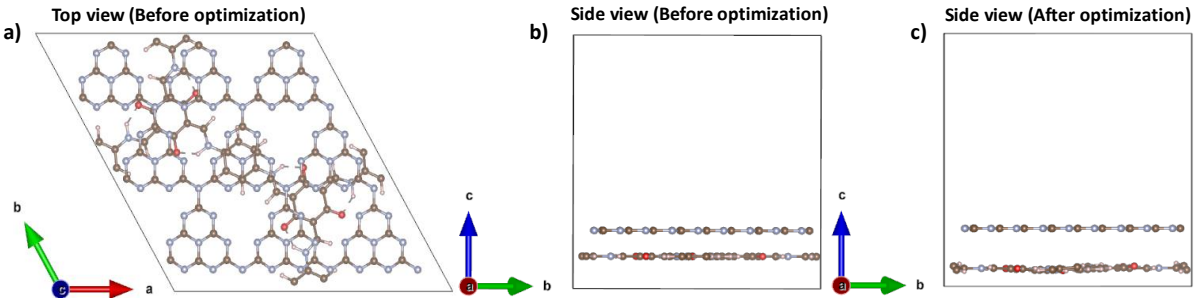

Figure S39. **Tp-Pa/gC_3N_4** heterostructure before optimization a) top view, b) side view. c) side view of **Tp-Pa/gC_3N_4** heterostructure after optimization.

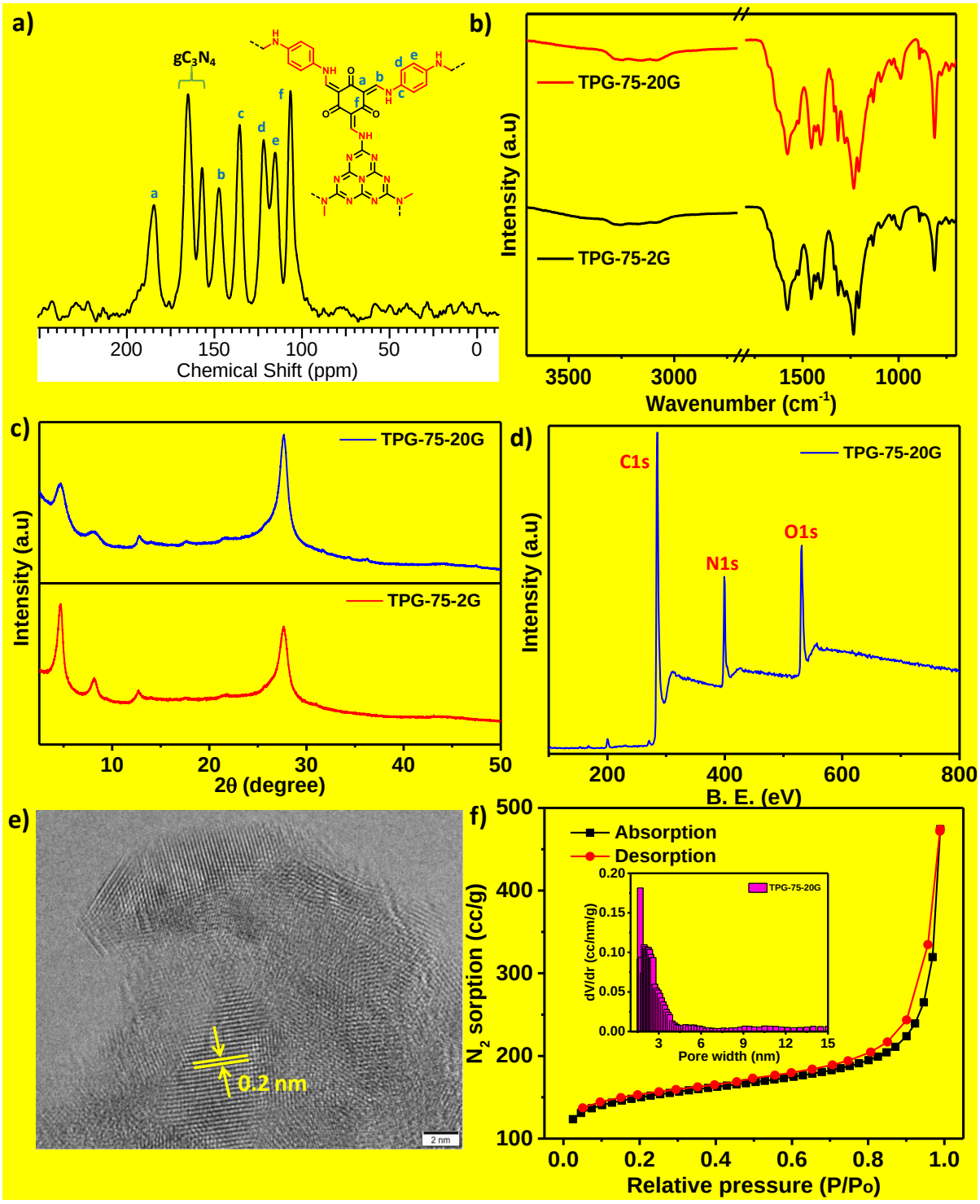

Figure S40. a) ^{13}C CP MAS NMR, b) FT-IR, c) PXRD, d) XPS, e) HR-TEM images showing fringes and d-spacing, and f) BET surface area (Pore size distribution as inset) of **TPG-75-20G** synthesized using planetary mixer.

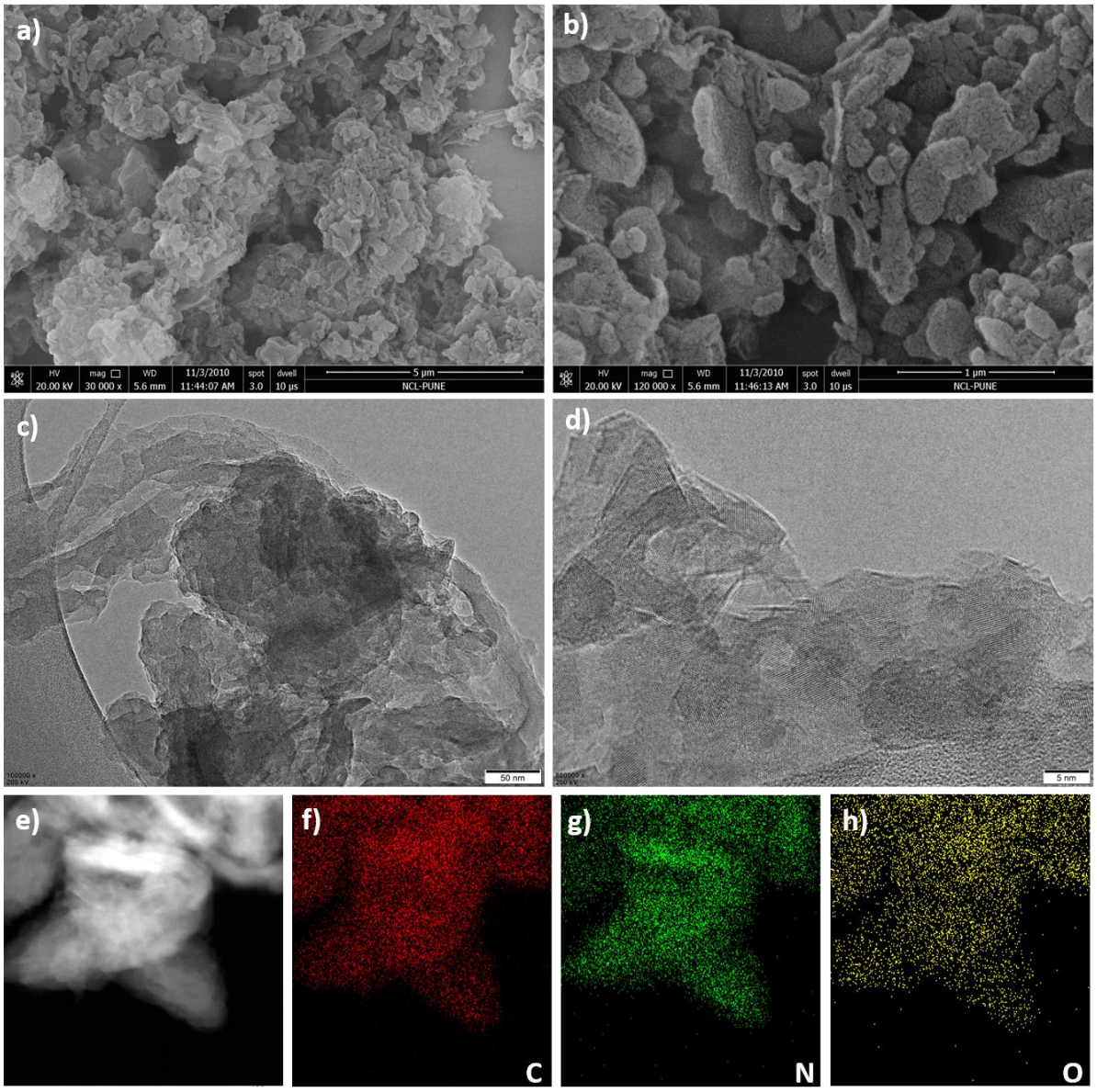

Figure S41. Electron microscopy characterisations of **TPG-75-20G** a,b) FE-SEM images. c,d) HR-TEM images. e-h) STEM elemental mapping showing overlay, C, N, O respectively.

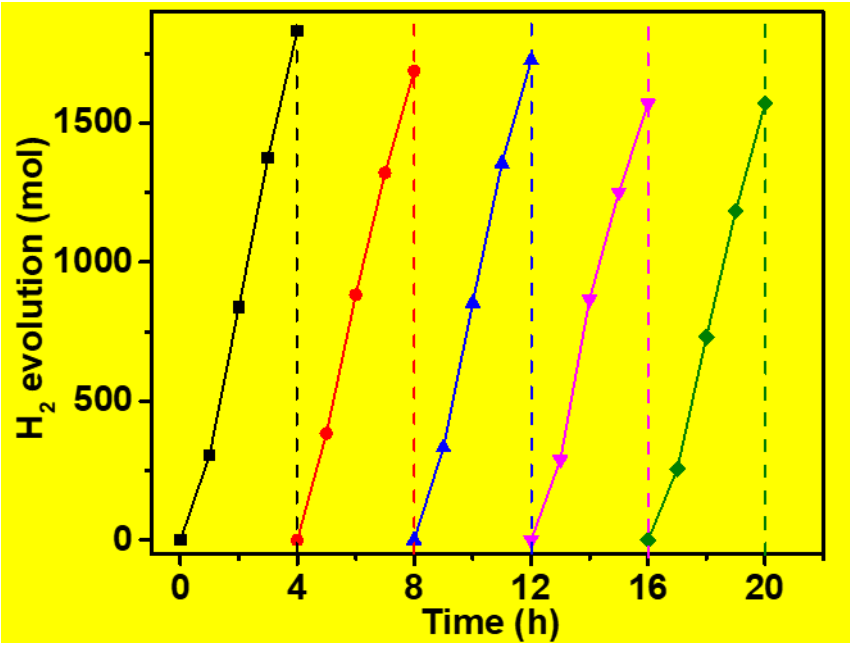

Figure S42. Cyclic stability of the PHE of **TPG-75-20G** with deionized water up to 5 cycles.

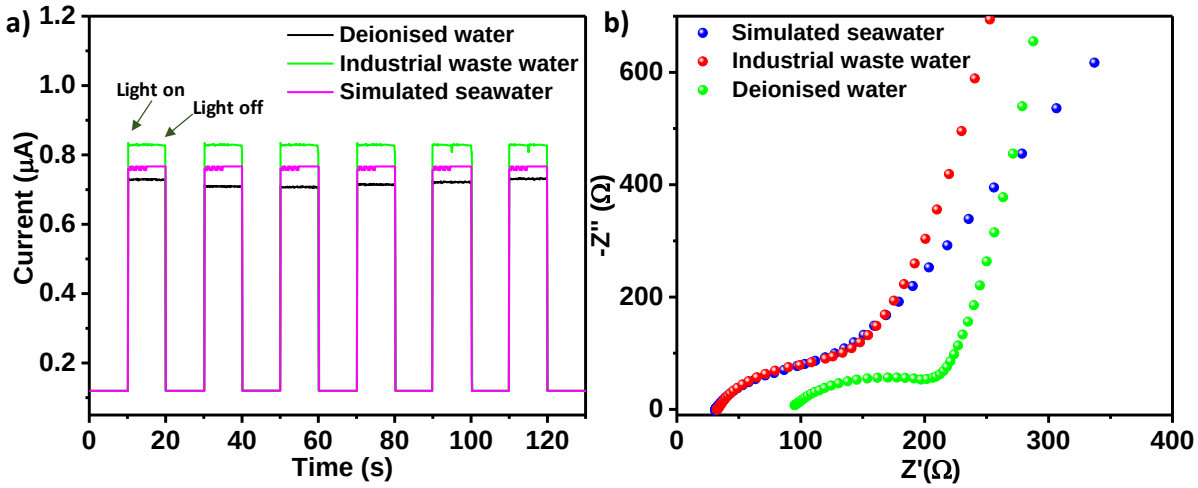

Figure S43. a) Photocurrent response and b) EIS studies of **TPG-75-20G** in water sources.

Tables

Table S1. Steps followed for the synthesis of **TPG-75-20G**.

Sr. No	Step	rpm	Time (minutes)
1.	**PTSA+ Pa**	1500	10
2.	**Tp**	1500	10
3.	**H_2O (20 mL)**	1000	10
4.	**gC_3N_4 (0.5 part) + H_2O (30 mL)**	1000	10
5.	**gC_3N_4 (0.5 part)**	1000	10
6.	**H_2O (5 mL)**	1000	10
7.	--	1000	10
8.	--	1000	5

Table S2. Comparison of HER reported for different 2D polymer organic photocatalyst and their performance.

Sr. No	COF	Co-Catalyst	SED	solvent	Irradiation	Activity (μmol/g/h)	AQE	Ref
1.	TPG-75	PVP-Pt NP	Ascorbic acid	H_2O	420	86,246	10.4 % at 450 nm	Our work
2.	TPG-75	PVP-Pt NP	Ascorbic acid	H_2O	AM 1.5	1,79,064		Our work
3.	TFPT-COF (20 mg)		10 vol% TEOA	H_2O	>420	1,970	2.2-3.9 % at 500 nm	*Chem. Sci.* **2014**, *5*, 2789-2793
4.	N2 COF (5 mg)	Co-1[b]	0.075 M TEOA (pH=8)	4:1 CAN/H2O	AM 1.5	782	0.16 % at 400 nm	*J. Am. Chem. Soc.* **2017**, *139*, 16228-16234
5.	FS-COF+WS5F (5 mg)	8 % Pt	Ascorbic acid	Water	>400 nm	16,300	0.6 % at 600	*Nat. Chem.* **2018**, *10*, 1180-1189
6.	Sp^2-COF_{ERDN}	3 % Pt	10 vol% TEOA	H_2O	>400 nm	2,120	-	*Chem* **2019**, *5*, 1632-1647
7.	A-TEBPY-COF (10 mg)	3 Wt% Pt	10 vol% TEOA	Phosphate buffer	AM 1.5	98	-	*Adv. Energy Mater.* **2018**, 8, 1703278
8.	N_3 COF (5 mg)	3 Wt% Pt	0.074 M TEOA (pH=7)	Phosphate buffer	>420 nm	1,703	0.44 % at 450 nm	*Nat. Comm.* **2015,** *6*, 8508
9.	TP-BDDA COF (10 mg)	3 % Pt	10 vol% TEOA	H_2O	>395 nm	330	1.3 % at 420 nm; 1.8 % at 520 nm	*J. Am. Chem. Soc.* **2018**, *140*, 1423-1427.
10.	TP-COF	6 % Pt	0.054 M Ascorbic acid	H_2O	>400 nm	8,420	0.4 % at 475 nm	*Angew. Chem. Int. Ed.* **2019**, 58, 18290-18294
11.	g-$C_{54}N_6$-COF	3 wt% Pt	10 mL TEOA	H_2O	420 nm	25,189		*Angew. Chem. Int. Ed.* **2020**, 59, 23845-23853
12.	COF–alkene	3 wt% Pt	TEOA	H_2O	420 nm	2,330	6.7 % at 420 nm	*Adv. Sci*. **2020**, *7*, 1902988
13.	PyTA-BC	7.4 wt% Pt	Ascorbic acid	H_2O with Methanol	420	5,030	1.46 % at 420 nm	*Adv. Optical Mater.* **2020**, 2000641
14.	BtCOF150	1 wt% Pt	TEOA	H_2O	420	750	0.2 % at 420 nm	*J. Am. Chem. Soc.* **2020**, 142, 9752-9762
15.	NKCOF-108	5 wt% Pt	Ascorbic acid	H2O	420	12,000	2.96% at 520 nm	*ACS Catal.* **2021**, 11, 2098−2107
16.	Tp-2C/BPy^{2+}-COF	3 wt% Pt	Ascorbic acid	H2O	420	34,600	6.93% at 420	*Angew. Chem. Int. Ed.* **2021**, 60, 9642-9649
17.	TtaTfa	8 wt% Pt	Ascorbic acid	H2O	420	20,700	1.43 % at 450 nm	*Angew. Chem. Int. Ed.* **2021**, 60, 19797-19803
18.	BDF-TAPT-COF (10mg)	8 wt% Pt	Ascorbic acid	H2O	AM 1.5	1,390	7.8 % at 420 nm	*Chem. Commun.*, **2021**, 57, 4464-4467
19.	ZnPor-DETH-COF (2.5 mg)	8 wt% Pt	TEOA	Phosphate buffer	420	413	0.063% at 450	*Nat. Commun.*, 12, **2021**, 1354.
20.	TTAN-COF	3 wt% Pt	Ascorbic acid	H2O	420	11,940		*ACS Catal.* **2022**, 12, 10718-10726
21.	Tz-COF-3 (10 mg)	3 wt% Pt	Ascorbic acid	H2O	420	43,200	6.9% at 420	*ACS Catal.* **2022**, 12, 9494−9502
22.	BDTCTF-1 (20 mg)	3 wt% Pt	TEOA	H2O	420	4,500	3.9% at 420	*ACS Appl. Energy Mater.* **2023**, 6, 930-938
23.	Tp-2C/BPy^{2+}-COF	3 wt% Pt	Ascorbic acid	H2O	420	34,600	6.93% at 420	*Angew. Chem. Int. Ed.* **2021**, 60, 9642-9649

24.	**COF-923-AC (5 mg)**	3 wt% Pt	Ascorbic acid	H2O	350	23,400	0.68% at 450	*Angew. Chem. Int. Ed.* **2023**, 62, e202216073
25.	**COF-JLU100 (5mg)**	12 wt% Pt	TEOA	H2O	420	1,07,380	4.27% at 420	*Angew. Chem.* **2022,** e202208919
26.	**PY-DHBD-COF (10 mg)**	3 wt% Pt	Ascorbic acid	H2O	420	71,160	8.4% at 420	*Nat. Commun.*, 13, **2022**, 1355.
27.	**TpPa(Δ)-Cu(II)-COF/L-cysteine**	-	L cysteine	H2O	420	14,720	0.78% at 600	*Nat. Commun.*, 13, **2022**, 5768.
28.	**TpPa-1-COF (10mg)**	Ni12P5	Ascorbic acid	H2O	420	3,160	-	*Small*, **2022,** 18, 2201340
29.	**BTT-BPy-PCOF(AC) (10 mg)**	3 wt% Pt	Ascorbic acid	H2O	420	15,800	3.06 % at 450	*Angew. Chem.Int. Ed.* **2023**, 62, e202300224
30.	**TP-COF (5 mg)**	8 wt % Pt	TEOA	H2O	420	29,120	13.48 % at 450	*Sci. China Mater.*, **2023**, 66, 2283-2289
31.	**COF-JLU35 (5 mg)**	1 wt% Pt	Ascorbic acid	H2O	420	70,800	3.21 % at 500	*J. Am. Chem. Soc.* **2023,** 145, 8364-8374
32.	**TpBpy-Ni2% (10 mg)**	3 wt% Pt	Ascorbic acid	H2O	420	72,800	5.3 % at 475	*Angew. Chem.Int. Ed.* **2023,** 135, e202217527
33.	**1 wt % Pd @ CTF-N**	1 wt% Pd	10 mL TEOA	H_2O	420 nm	10,556		*ACS Appl. Mater. Interfaces*, **2020**, 12, 12774−12782
34.	**CTF-7 (5 mg)**	1 wt% Pd	10 mL TEOA	H2O	420	9,240		*Chem.Commun.*, 2022, 58, 92-95
35.	**T3N-CTF**	3 wt% Pt	TEOA	H2O	420	6,485	12.2% at 405	*Chem.Sus.Chem.*, **2022,** 15, e202200828
36.	**CTF-NWU-1**	3 wt% Pt	TEOA	H2O	420	17,600	0.20 % at 420	*J. Mater. Chem. A*, **2022**,10, 16328-16336
37.	**BDTCTF- 1 (20 mg)**	3 wt% Pt	TEOA	H2O	420	4,500	3.9 % at 420	*ACS Appl. Energy Mater.* **2023,** 6, 930-938
38.	**NH_2-UiO-66/TpPa-1-COF (10 mg)**	3 % Pt	Sodium Ascorbate	Phosphate buffer	>420 nm	23,410	-	*Angew. Chem. Int. Ed.* **2018**, 57, 12106-12110
39.	**NH_2-UiO-66/TpPa-1-COF**	3 wt% Pt	Ascorbic acid	Buffer (PH 7)	420	14,228	9.75 % at 500	*J. Am. Chem. Soc.* **2020**, 142, 4862-4871
40.	**a-Fe2O3/TpPa-2-COF (3 : 7)**	-	Sodium Ascorbate	H_2O	420	3,770	0.137 % at 450 nm	*J. Mater. Chem. A*, **2020**, 8, 4334-4340
41.	**rGO(5%)–TpPa-1-COF**	3 wt% Pt	Sodium ascorbate	H_2O	420	11,980	7.53 % at 450 nm	*J. Mater. Chem. A*, **2020**, 8, 8949-8956
42.	**CTF-1/GO-3.0 (10 mg)**	3 wt% Pt	TEOA	H_2O	420	2262	-	*Chem. Eur. J.* **2021,** 27, 13059–13066
43.	**2.5-TBTA/g-C3N4**	2.08 wt% Pt	Ascorbic acid	H_2O	420	26,040	-	*Catal.. Sci.. Technol.*, **2021**, 11, 2616-2621
44.	**Pd0.033/TPTTA/ SiO2**	Pd	Ascorbic acid	H_2O	420	156 mmol h^{-1} g_{COF}^{-1}	7.3% at 420	*ACS Appl. Mater. Interfaces*, **2022,** 14, 5, 6885-6893
45.	**Zn@HTpPa (10 mg)**	3 wt% Pt	Sodium ascorbate	Phosphate buffer	420	28,000	-	*Chem. Cat. .Chem.*, **2022**, 14, e202101800
46.	**ZT-5 (10 mg)**	-	10 vol% furfuryl alcohol	H_2O	420	9,730	13.91 % at 500	*J. Mater. Chem. A*, **2022,** 10, 22531-22539
47.	**TT-TAB (1 mg)**	3 wt% Pt	Ascorbic acid	H_2O	395	1,13,900	4.48% at 415	DOI:10.26434/chemrxiv-2021-q1b4b-v2
48.	**P2CNNS (20 mg)**	-	Ascorbic acid	H_2O/DMF	420	50,200	-	*Applied Surface Science*, **2023**, 615, 156414
49.	**$[Mo_3S_{13}]_2$–@ZnP-Pz-PEO-COF (10 mg)**	-	15 vol% lactic acid	H_2O	420	11,000	3.6 % at 600	*Nat. Commun.*, **2023**, 14, 329

50.	**Mo_3S_{13}@EB-COF**		Ascorbic acid	DMF/H2O (1:1)	420	13,215	4.49 % at 475	*Chem. Commun.*, **2018**, 54, 13563—13566.
51.	**MoS_2-3%/TpPa-1-COF**		Ascorbic acid	H_2O	420	5,580	0.76 % at 420	*J. Mater. Chem. A*, **2019**, 7, 20193–20200
52.	**MOF-808@Tp-Pa-1-COF(6/4)**	3 wt% Pt	Sodium Ascorbate	H_2O	420	11,800		*J. Mater. Chem. A*, **2021**, 9, 16743–16750
53.	**30%PEG@BT-COF**	5 wt% Pt	Ascorbic acid	H_2O	420	11,140	11.2 % at 420	*Nat. Commun.*, ***2021***, *12*, *3934*
54.	**12.5% Ni12P5/TpPa 1-COF**		Ascorbic acid	H_2O	420	3,160		*Small*, **2022**, 18, 2201340
55.	**MTV-Ti-MOF/COF**	1.2 wt% Pt	Ascorbic acid	PBS Buffer	420	13,980	5.9% at 515	*Angew.Chem.Int.Ed.***2022**,61,e202114071
56.	**TiO2-x/TpPa-1-COF (6:4)**	3 wt% Pt	Sodium Ascorbate	PBS Buffer	420	15,330	6.7% at 420	*Chem. Eng. J.*, **2022**, 446,137213
57.	**PTCOF-OID**	3 wt% Pt	Sodium Ascorbate	H_2O	420	29,290	2.51% at 420	*Adv. Funct. Mater.***2023**,33, 2307300
58.	**Cu2O/PyTTA-TPA COFs**		Methanol	H_2O	420	12,500	21.5% at 475	*ACS Nano*, **2023**, 17, 5994−6001

Table S3. Types of water and properties.

No	**Type of Water**	**Composition**	**pH**
1	Deionized water	Pure	7.79
2	Simulated seawater	NaCl, $MgCl_2$, $MgSO_4$, $CaSO_4$, K_2SO_4, K_2CO_3, $MgBr_2$	7.79
3	Industrial wastewater	Formic acid, propionic acid, butyric acid	3.26
4	Processed seawater	Chloride, sulphate, iron, sodium, silicon, potassium, magnesium, calcium, copper	7.65

Table S4. Photoluminescence emission properties of **gC_3N_4**, **Tp-Pa**, and **TPG-75**.

Catalyst	**Lifetime (ns)**	**Contribution (%)**	**CHISQ**
gC_3N_4	7.7	44.86	1.22
	42.1	17.6	
	1.9	37.54	
TPG-75	0.53	73.31	1.09
	3.66	26.69	
Tp-Pa	0.18	100	1.03

Table S5. Photoluminescence emission properties of **gC_3N_4**, and **gC_3N_4** mixed with different ratios of **Tp-Pa**.

Catalyst	Lifetime (ns)	Contribution (%)	CHISQ
gC_3N_4	7.7	44.86	1.22
	42.1	17.6	
	1.9	37.54	
gC_3N_4:Tp-Pa::100:0.1	6.7	44.06	1.18
	43.02	13.46	
	1.57	42.48	
gC_3N_4:Tp-Pa 100:0.5	6.65	44.02	1.22
	41.2	13.56	
	1.53	42.42	
gC_3N_4:Tp-Pa 100:1	6.8	46.58	1.22
	43.07	14.48	
	1.59	38.94	
gC_3N_4:Tp-Pa 100:5	5.8	45.66	1.12
	38.62	13.29	
	1.24	41.05	

Table S6. Comparison of HER reported for different photocatalyst and their performance from seawater.

Sr. No	Catalyst	Co-Catalyst	SED	solvent	Irradiation	Activity (µmol/g/h)	Reference
1.	**TPG-75**	PVP-Pt NP	Ascorbic acid	H_2O	420	1,09,125	Our work
2.	**COP-$TP_{3:1}$**	3 wt% Pt	TEOA	3wt% NaCl	420	5200	*ACS Appl. Mater. Interfaces.* **2018**, 10, 30698−30705
3.	**COP-TF@CNi_2P**	CNi2P	0.2 M Na_2S/$NaSO_3$	seawater	400	2500	*ACS Appl. Mater. Interfaces*, **2019**, 11, 41313-41320
4.	**PFNH-Br**		triethylamine	seawater	Simulated solar light	1806	*Adv. Energy Sustainability Res.***2022**,3, 2200068
5.	**Tp-Pa**	0.5Wt% Pt	0.1M Ascorbic acid	Simulated seawater	420	41,300	*Nano Research*, **2023,** 16, 6251-6259
6.	**TTR-COF**	Au	Triethanolamine	seawater	420	141	*ACS Sustainable Chem. Eng*., **2019**, 7, 18574-18581
7.	**gC_3N_4**	Pt	Glycerol	seawater	Simulated solar light	847	*Int. J. Hydrogen Energy* **2018**, *43*, 14925-14933.
8.	**PorFn**	Pt	TEOA	0.5M NaCl	420	10,800	*Adv. Funct. Mater.* **2019**, 29, 1808156
9.	**CTF-HUST-3**		TEOA	3wt% NaCl	Visible light	812	*Chem. Mater.* **2021**, *33*, 1994-2003

10.	**o-CND-2**		TEOA	seawater	420	19,700	*J. Am. Chem. Soc.* **2021,** *143*, 20122-20132
11.	**V_{Ti}-TiO2**	0.75 wt% Pt	Methanol	Simulated seawater	420	25,900	*Chemistry* **2021**, *27*, 14202-14208.
12.	**$ZnS_{1-x-0.5y}O_x(OH)_y$-ZnO**		Na_2SO_3/Na_2S	3mol/L NaCl	Visible light	18.3	*Int. J. Hydrogen Energy* **2011**, *36*, 10565-10573
13.	**SiO_2/Ag@TiO_2**		Glycerol	Simulated seawater	365	800	*Energy Environ. Sci.*, **2016**, 9, 3151-3160
14.	**Pt-TiO_2**	Pt	Methanol	seawater	320	1,573	*Catal. Commun.* **2018**, *114*, 124-128.
15.	**CDs/CdS-S**	CD	10 % Lactic acid	seawater	420	4,660	*Appl. Catal., B* **2019**, *242*, 178–185
16.	**Ti–O–Si (400)**	/	10 vol% TEOA	5 wt% NaCl	solar light	1930.5	*Nanoscale*, **2018**, 10, 2275-2284.
17.	**WS_2/C-TiO_2/g-C_3N_4**	3 wt% Pt	10 vol% triethanolamine	seawater	420	1200	*ChemSusChem*., **2018**, 11, 4077-4085
18.	**H-CoS/CdS-2**		Na_2S/Na_2SO_3	Simulated seawater	420	143.1	*Int. J. Hydrogen Energy*, **2022**, 47, 9220-9229.
19.	**Ti3C_2/$Cd_{0.5}Zn_{0.5}S$**	Ti_3C_2	Na_2SO_3/Na_2S		420	9071	*Appl. Mater. Today,* **2021**, *22*, 100926.
20.	**P-8CE**	Pt	TEA	Natural seawater	420	38,900	*Adv. Energy Mater.* ***2023,*** *2300986*

References

S1 Kresse, G.; Furthmüller, J. Efficiency of Ab-Initio Total Energy Calculations for Metals and Semiconductors Using a Plane-Wave Basis Set. *Comput. Mater. Sci*. **1996**, *6* (1), 15–50.

S2 Perdew, J. P.; Burke, K.; Ernzerhof, M. Generalized Gradient Approximation Made Simple. *Phys. Rev. Lett*. **1996**, *77* (18), 3865–3868.

S3 Grimme, S. Semiempirical GGA-type Density Functional Constructed with a Long-range Dispersion Correction. *J Comput. Chem*. **2006**, *27* (15), 1787–1799.

S4 Huang, C.; Illiassou, B.; T-Raissi, A.; Muradov, N. Preparation of High Efficiency Visible Light Activated Pt/CdS Photocatalyst for Solar Hydrogen Production; Guo, J., Ed.; San Diego, CA, 2007; p 665010.

S5 Martin, D. J.; Qiu, K.; Shevlin, S. A.; Handoko, A. D.; Chen, X.; Guo, Z.; Tang, J. Highly Efficient Photocatalytic H_2 Evolution from Water Using Visible Light and Structure-Controlled Graphitic Carbon Nitride. *Angew. Chem. Int. Ed.* **2014**, *53* (35), 9240–9245.